

UNIVERSITY *of* WASHINGTON

SAILFIN

DBF'23



## Contents

<b>1 Executive Summary</b>	<b>4</b>
<b>2 Management Summary</b>	<b>5</b>
2.1 Team Organization . . . . .	5
2.2 Milestone Chart . . . . .	5
<b>3 Conceptual Design</b>	<b>6</b>
3.1 Mission Requirements and Constraints . . . . .	6
3.2 System and Sub-system Requirements . . . . .	9
3.3 Sensitivity Analysis . . . . .	10
3.4 Configuration Selection . . . . .	11
3.5 Final Conceptual Design Configuration . . . . .	14
<b>4 Preliminary Design</b>	<b>15</b>
4.1 Design Methodology . . . . .	15
4.2 Design and Sizing Trade Studies . . . . .	16
4.3 Aircraft Stability Analysis . . . . .	20
4.4 Aircraft Performance Analysis . . . . .	22
4.5 Environmental Uncertainties . . . . .	26
4.6 Predicted Aircraft Mission Performance . . . . .	27
<b>5 Detailed Design</b>	<b>27</b>
5.1 Dimensional Parameters . . . . .	27
5.2 Structure Characteristics and Capabilities . . . . .	28
5.3 Sub-system Design . . . . .	29
5.4 Weight and Balance . . . . .	37
5.5 Predicted Aircraft Flight and Mission Performance . . . . .	38
5.6 Drawing Package . . . . .	38
<b>6 Manufacturing Plan</b>	<b>43</b>
6.1 Manufacturing Processes Descriptions . . . . .	43
6.2 Manufacturing Overview . . . . .	45
6.3 Manufacturing Schedule . . . . .	48
<b>7 Test Plan</b>	<b>48</b>
7.1 Test Schedule . . . . .	49
7.2 Testing Objectives . . . . .	49
7.3 Design Analysis Testing . . . . .	49
7.4 Flight Tests . . . . .	51
<b>8 Performance Results</b>	<b>55</b>
8.1 Demonstrated System Performance . . . . .	55
8.2 Flight Performance . . . . .	57
<b>9 References</b>	<b>60</b>

## Abbreviations, Acronyms, and Symbols

- ABS: Acrylonitrile Butadiene Styrene
- ac: Aerodynamic Center
- APC: Advanced Precision Composites Propeller Company
- APD: Advanced Power Drives
- AVL: Athena Vortex Lattice
- $A_t$ : Length of the Antenna
- $b$ : Wing Span
- $t$ : Thickness
- BWB: Blended Wing Body
- $c$ : Chord Length
- CAD: Computer Aided Design
- CFD: Computational Fluid Dynamics
- CFRP: Carbon Fiber Reinforced Plastic
- CG: Center of Gravity
- $C_L$ : Coefficient of Lift
- $C_M$ : Coefficient of Moment about the AC
- CNC: Computer Numerical Control
- $D$ : Drag Force
- $d$ : Antenna Diameter
- $C_D$ : Coefficient of Drag
- $\epsilon$ : Oswald's Efficiency
- FEA: Finite Element Analysis
- FoS: Factor of Safety
- $g$ : Gravitational Acceleration
- GM: Ground Mission
- $I$ : Electric Current
- $L$ : Lift Force
- LiPo: Lithium-Polymer (often refers to batteries)
- M1: Mission 1
- M2: Mission 2
- M3: Mission 3
- $n$ : Lift to Weight Ratio
- $P_{prop}$ : Propulsion Power
- $P$ : Structural Applied Load
- PDB: Power Distribution Board
- PETG: Polyethylene Terephthalate Glycol
- PLA: Polylactic Acid
- $q$ : Dynamic Pressure
- $Q$ : First Moment of Area
- $R_{sys}$ : System Electrical Resistance
- RPM: Revolutions Per Minute
- $T$ : Thrust
- $\tau$ : Shear Stress
- $t_{est}$ : Estimated Flight Time
- TO: Topology Optimization
- TOFL: Takeoff Field Length
- TPU: Thermoplastic Polyurethane
- UW: University of Washington
- $V$ : Voltage
- $v$ : Velocity
- $W$ : Weight
- XPS: Extruded Polystyrene
- $\alpha$ : Angle of Attack (AOA)
- $\theta$ : Bank Angle

## 1 Executive Summary

This report details the design, manufacturing, and testing of the University of Washington's aircraft for entry in the 2023 American Institute of Aeronautics and Astronautics (AIAA) Design Build Fly (DBF) competition. Team HuskyWorks designed an aircraft, titled the *UW-23 Sailfin*, to complete three flight missions and one ground mission per the requirements given by the AIAA. To maximize all mission scores, the team designed the *Sailfin* to maximize payload weight for M2, maximize antenna length for M3, maximize strength-to-weight for GM, and minimize aircraft assembly time. Based on mission requirements, the team identified speed, assembly time, and strength-to-weight to be the critical factors in design. Team HuskyWorks followed an iterative design process to improve upon and optimize each aircraft component.

The *UW-23 Sailfin*, shown in Fig. 1, is a single-engine, low-wing taildragger with a conventional tail and a tapered empennage. A single engine was selected because it provides adequate thrust for all flight missions, while reducing weight and increasing propulsive efficiency. A taildragger was selected to provide a positive angle of attack on takeoff. A flat bottomed fuselage was selected to increase shipping container packing efficiency, with a tapered empennage to save weight and streamline the aircraft's body. A low wing was selected to allow for easy access to the payload and electronics. Due to the need to assemble the aircraft quickly before each flight, the *Sailfin* was designed with minimal connection points. The *Sailfin* was constructed from various carbon fiber composite structures, improving the strength-to-weight ratio of the aircraft, and improving structural capabilities. The team designed and built custom wing spars to optimize the structure for both ground and flight load conditions. A mount for the M3 antenna was designed to minimize aerodynamic disturbance at the root and maximize antenna length. A test stand for ground mission was designed to have a pinned-pinned connection to minimize bending stress at the wing tips.

To maximize mission scores, the team completed a sensitivity analysis to determine the M2 payload and M3 antenna length. The *UW-23 Sailfin* is predicted to complete 14 laps in 10 minutes in M2, carrying 9.33 lb of payload. M3 is predicted to be completed in 87 seconds with an antenna that is 39 in long. The sensitivity analysis yielded the M2 payload value, and indicated that maximizing antenna length was optimal for M3. Due to the size constraints on the shipping container, the antenna was sized based on the maximum length that could fit. The maximum cruising speed is 131 ft/s in M3, with a cruise speed of 92 ft/s in M2. During ground mission, the aircraft will be loaded with 200 lb. Competition mission simulations have been flown to validate predicted performance. Testing has proven the aircraft is capable of flying all three missions.

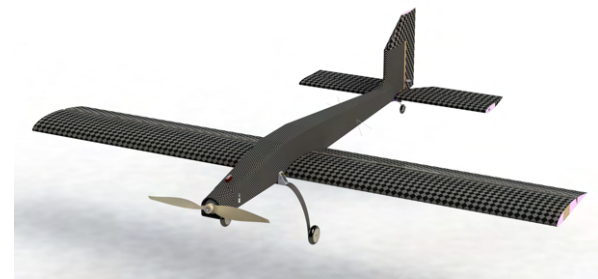


Figure 1: *UW-23 Sailfin*

## 2 Management Summary

The HuskyWorks team has 79 total members consisting of 27% seniors, 19% juniors, 20% sophomores, 30% freshmen and 4% graduate students. 13 elected officials lead unique aspects of the design process and club operations. The club is funded, supported, and advised by 25 sponsors including: T-Motor, Ansys, SolidWorks, The Boeing Company, and Marymoor R/C Club.

### 2.1 Team Organization

The HuskyWorks team is divided into 5 main sub-teams, each responsible for a different discipline of the project. Each sub-team has a number of technical projects that contribute to the development of individual parts of the aircraft. The overall organization is jointly overseen by the Project Manager and the Chief Engineer. The Project Manager facilitates the scheduling of project timelines and deadlines while cultivating cross-team communication. The Chief Engineer defines design constraints and oversees design, analysis, and integration definition. The Business Lead manages procurement, fundraising, marketing, and budgeting. The Manufacturing Lead is responsible for overseeing the production of the aircraft. The Chief Pilot is responsible for flight test, ground support and the fly off activities. The HuskyWorks team is also advised by one faculty member who reviews designs and approves testing activities. All individual technical disciplines are run by a sub-team lead, who manages a portfolio of technical projects that pertain to their area of expertise. Every team member is assigned to at least one specific technical project under a sub-team and is tasked with designing components, performing analyses, and contributing to manufacturing.

### 2.2 Milestone Chart

Gantt charts were used to manage club operations, deadlines, and milestones. High-level charts were used for broad design management, integration, and administrative deadlines. Additionally, they provided a general overview of all major tasks across the project's lifecycle while low-level charts focused on sub-task milestones and component deadlines. Figure 3 shows the high-level Gantt chart used during the 2022-23 competition cycle.

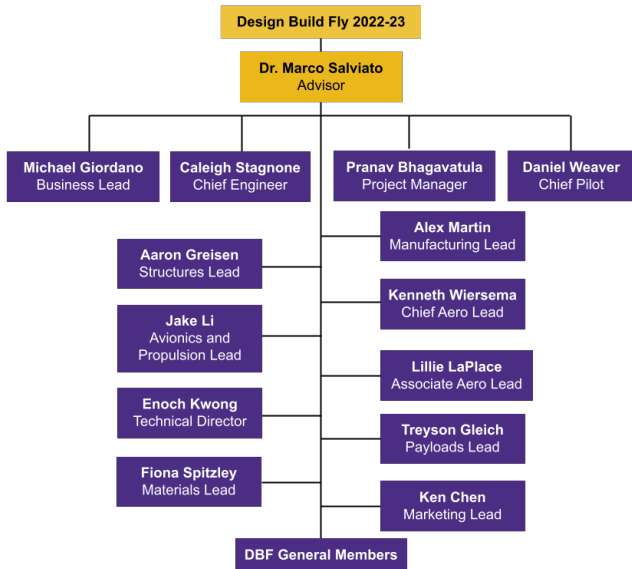


Figure 2: Team Organizational Chart

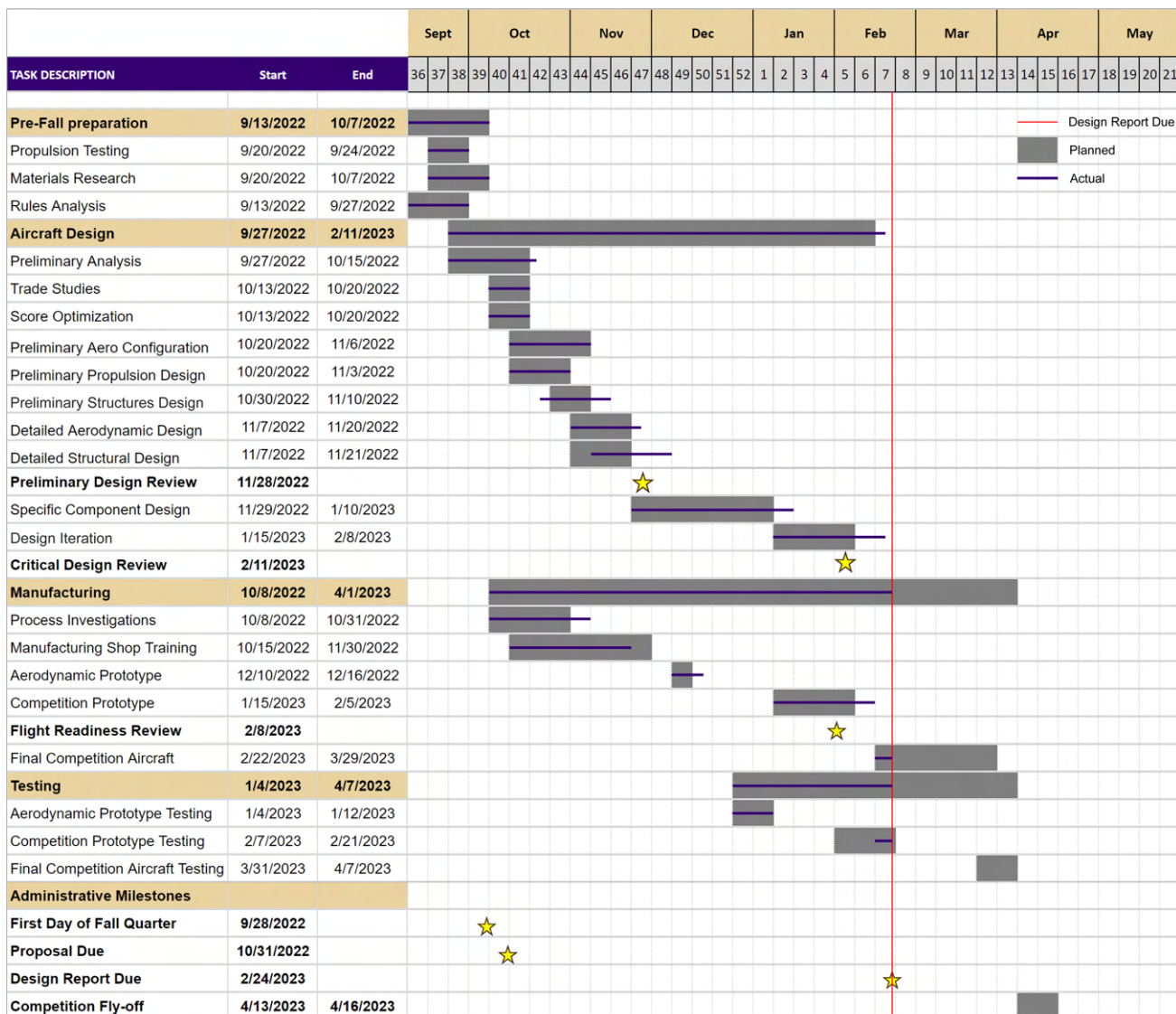


Figure 3: Team Gantt Chart

### 3 Conceptual Design

In selecting a configuration, rules and requirements were analyzed and allocated into sub-system requirements. Then, environmental uncertainties were considered based on the differences in climates between Seattle and Tucson. Next, a sensitivity analysis was performed to highlight which characteristics had the greatest impact on the final score. These characteristics were then analyzed through trade studies, which led to the selection of the final configuration for the *Sailfin*.

#### 3.1 Mission Requirements and Constraints

The total score is determined by the product of the written report score and the total mission score with a maximum of 3 added participation points. A single participation point will be awarded for each of the following:

attending the fly-off, completing tech inspection, and attempting a flight mission. The total mission score will be the sum of the three flight missions and the ground mission performance scores.

$$\text{Total Score} = \text{Written Report Score} \cdot \text{Total Mission Score} + P \quad (1)$$

Table 1: Participation Scoring

P	Participation
1	Attending the Fly-off
2	Completing Tech Inspection
3	Attempting a Flight Mission

$$\text{Total Mission Score} = M1 + M2 + M3 + GM \quad (2)$$

### 3.1.1 Staging

Before each mission, all aircraft components and payloads will be in the shipping box within the staging area. Only three people are allowed in the staging area: the assembly crew member, the pilot, and an observer. The only person allowed to touch the aircraft in the staging box is the assembly crew member. The assembly must be completed in less than 5 minutes, including all electrical connections and battery placements. The aircraft must be ready to fly before being called to the flight line except for the insertion of the arming plug. If the team forgets a crucial component that requires leaving the staging area to retrieve it, the flight attempt is forfeited. For each mission, a coin will be flipped, determining which wing will be used, once for each side, as shown in Table 2. Time for a mission is started when the throttle is advanced for the first takeoff attempt. All flight missions require takeoff within 60 ft. Should the aircraft not make this distance, it must land and reattempt takeoff.

Table 2: Wing Selection Process

Coin Flip	Wing Selection
Heads	"L1" or "R1"
Tails	"L2" or "R2"

Each flight mission will be flown according to the lap configuration shown in Fig. 4. Three laps will be flown for M1 and M3, while for M2, as many laps as possible will be flown within 10 minutes.

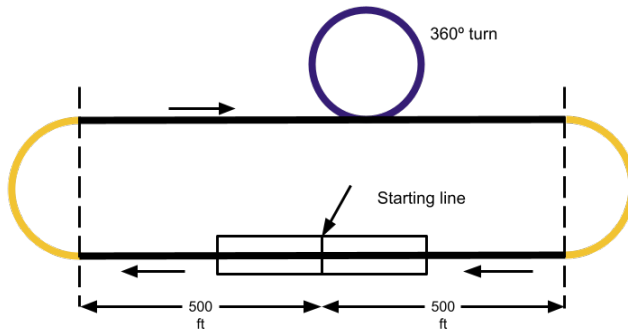


Figure 4: Competition Lap Layout

### 3.1.2 Ground Mission

The GM can be attempted at any time throughout the competition. At the beginning of the attempt, all aircraft components and payloads must be stored in the shipping box. A coin will be flipped twice to determine which wings are used. During the mission, only the assembly crew member may touch aircraft components and payloads. First, the heaviest aircraft configuration, as declared at tech inspection, will be assembled and verified. Next, the pilot will verify that all flight controls are working properly. The aircraft will then be attached to the ground test fixture and weights will be applied to the center of the fuselage, inboard of the wing attachment. The final weight must hold for 30 seconds, and the pilot must once again confirm that the flight controls are working. There will be a 10 minute window to complete the assembly and the application of weights.

$$GM = \left[ \frac{N_{(\text{total test weight} / \text{max aircraft weight})}}{\text{Max}_{(\text{total test weight} / \text{max aircraft weight})}} \right] \quad (3)$$

### 3.1.3 Mission 1

M1 requires no payload, and is simply a proof of flight. To successfully complete the mission, the aircraft must complete 3 laps within a 5 minute window. Landing is not included in this window, but the aircraft must complete a successful landing to receive a score. Teams receive 1 point upon successful completion of M1.

### 3.1.4 Mission 2

M2 is scored based on the number of laps flown in a 10 minute window and the weight of the payload, referred to as the electronics package. The electronics package must have minimum dimensions of 3.00 in x 3.00 in x 6.00 in, and must be carried internally to the aircraft. The electronics package must make up 30% or greater of the gross aircraft weight. Similar to M1, landing is not included in the 10 minute window. The M2 score is given by Eq. 4, where  $\text{Max}_{(\text{payload weight} * \# \text{ laps flown})}$  is the highest  $(\text{payload weight} * \# \text{ laps flown})$  of all teams.

$$M2 = 1 + \left[ \frac{N_{(\text{payload weight} * \# \text{ laps flown})}}{\text{Max}_{(\text{payload weight} * \# \text{ laps flown})}} \right] \quad (4)$$

### 3.1.5 Mission 3

The payload for M3 is a jamming antenna. The antenna will be an unmodified  $\frac{1}{2}$  in Schedule 40 PVC pipe, in accordance with ASTM-D1785. The surface at the end of the pipe must be perpendicular to the antenna axis. Up to 3 antennas may be brought to competition. However, all antennas must be stored in the shipping container. In preparation for flight, the antenna will be mounted to the wingtip opposite the flight line upon takeoff. The antenna must be securely attached to the wingtip with two fasteners and an adapter. The antenna must not have internal or external supports beyond the extent of the adapter. The antenna must project vertically above the wing with no portion projecting below the lower surface of the wing. A counterweight of comparable size and shape to the antenna adapter may be placed on the wing opposite the antenna. This mission is scored based on the time it takes to fly three laps and the length of the antenna. The M3 score is given by Eq. 5, where antenna length is measured from the point the antenna exits the adapter to the top surface, and the  $\text{Max}_{(\text{antenna length} / \text{mission time})}$  is the highest (antenna length / mission time) of all teams.

$$M3 = 2 + \left[ \frac{N_{(\text{antenna length} / \text{mission time})}}{\text{Max}_{(\text{antenna length} / \text{mission time})}} \right] \quad (5)$$

## 3.2 System and Sub-system Requirements

Based on the AIAA 2023 Rules Document [1], Table 3 was developed. This table was constructed using five categories: one for each of the 4 competition missions, and one for the general requirements of all flight missions. In order for the aircraft to qualify for competition, each of the requirements will be verified.

### 3.2.1 Translation of Mission Requirements into Sub-system Requirements

Table 4 shows how the mission requirements in Table 3 translate into sub-system requirements. The Parent Requirement column indicates where the sub-system requirements were derived from. Some system requirements did not translate into sub-system requirements as they already encompass the extent of what is required. Additionally, specific values were not listed unless they were provided in the rules, as these were developed upon analysis of the rules.

Table 3: Mission Requirements and Constraints

System	Label	Mission Requirement
General Requirements	GR.1	The aircraft must be unmanned
	GR.2	The aircraft must takeoff within 60 ft
	GR.3	The propulsion battery must not exceed 100 W-hr of stored energy
	GR.4	The aircraft must fit disassembled within a box with a linear dimension no larger than 62.00"
	GR.5	The aircraft must be flown in the same flight configuration for all missions
	GR.6	The aircraft must be radio-controlled
	GR.7	The aircraft must be electric and propeller driven
	GR.8	The batteries must either NiCd/NiMH or LiPo
	GR.9	The aircraft must be assembled within 5 minutes before each mission
	GR.10	The box must contain two sets of identical wings
	GR.11	The aircraft, box, and extra set of wings must weigh less than 50 lb
	GR.12	The aircraft must have an external arming plug and avionics switch
Mission 1	M1.1	The aircraft must fly 3 laps within 5 minutes with no payload
Mission 2	M2.1	The aircraft must carry a payload equal to at least 30% of the aircraft weight
	M2.2	The payload must have minimum dimensions of 3.00" x 3.00" x 6.00"
	M2.3	The aircraft must fly as many laps as possible within a 10 minute window
Mission 3	M3.1	The aircraft must carry an unmodified ½" Schedule 40 PVC pipe antenna that extrudes vertically from the tip of the wing
	M3.2	The aircraft must fly 3 laps as fast as possible
	M3.3	The antenna must extrude above the tip of the wing
	M3.4	The antenna must be mounted at the tip of the wing
	M3.5	The aircraft will be scored based on antenna length and lap time
Ground Mission	GM.1	The aircraft must demonstrate its structural margin through a three point bending test
	GM.2	The ground mission must be completed within 10 minutes
	GM.3	The aircraft must be loaded to the maximum ground mission weight and hold the weight for 30 seconds
	GM.4	The aircraft must be capable of actuating all flight controls under the maximum ground mission weight
	GM.5	The aircraft must not undergo any permanent deformation
	GM.6	The aircraft will be scored based on weight applied and maximum gross aircraft weight

Table 4: Sub-System Requirements

Requirement Type	Parent Requirement	Sub-System Requirement
Aerodynamic Requirements	GR.4	The aircraft must be designed to conform to shipping container dimensions of L+W+H = 62 in
	GR.2 & M2.1	The aircraft must generate sufficient lift in all flight regimes
	M3.2	The aircraft configuration must minimize drag to allow for maximum possible speed
	M3.1	The aircraft configuration must have sufficient yaw authority for M3
Avionics & Propulsion	GR.2	The propulsion system must provide sufficient thrust to takeoff within 60 ft
	M1.1, M2.1 & M3.2	The propulsion system must provide sufficient thrust to overcome drag in all flight configurations
	M2.3	The propulsion system must have at least 10 minutes of endurance while maintaining optimum M2 flight speed
	GR.12	The avionics system must be easy to disable
Structures	M2.1 & M3.2	All structural components must be able to withstand maximum load cases in all flight regimes
	M3.1	The aircraft wing must be capable of withstanding the torsional effects of the antenna
	GM.3 & GM.5	The aircraft must be capable of withstanding a heavy point load without significant structural deformation
	GR.9	All aircraft components must be assembled in a maximum of 20 seconds
	GM.1 & GM.6	The aircraft must have a high strength to weight ratio

### 3.3 Sensitivity Analysis

#### 3.3.1 Score Analysis

To determine the primary design factors for this year's competition, a sensitivity analysis was performed based on constraints provided by the AIAA competition rules [1]. Initially, it was determined that the maximum an-

tenna length was fixed due to box dimensions. Through initial CFD simulations and an early flight test, the drag produced by the antenna was determined to not cause significant changes in lap time compared to environmental conditions or pilot handling. M3 then became a driver of the top speed of the aircraft. M2 was determined to have the greatest uncertainty in the potential scoring due to the conflicting objectives of both maximum range, in terms of laps flown, and payload mass carried. The variables under consideration for optimization were weight of the aircraft, cruise speed, and total flight time. The maximizing constraints for M2 were determined to be cruise speed greater than stall speed, 100 Wh of battery energy stored, and takeoff distance being less than 60 ft. A MATLAB script then maximized the M2 score based on the total number of laps flown. A system of equations was created based on these constraints and was fed into MATLAB's [2] optimization package to produce a total score for a baseline configuration based on previous years' aircraft. Each prior year's parameter was multiplied by a factor of 0.5 to 1.5 to generate a sensitivity analysis for M2. The plot in Fig. 5 shows the results of this process, visualizing how changes in parameters affect mission score. The plot indicates that the quantities to be maximized were thrust, maximum  $C_L$  and wing area of the aircraft, while keeping an AR of around 6 for maximum score gain. The parasitic drag was less sensitive, so minimizing wetted area was a lower priority. This score optimization script also calculated that the optimum M2 configuration had an average cruise velocity of 111 ft/s to reach 12 laps and a payload weight of 9.33 lb.

### 3.4 Configuration Selection

The following section details the design considerations made by the team throughout the conceptual design phase via weighted decision matrices. Each figure of merit was assigned a weight factor between 0 and 1 based on the impact each had on the final decision. A score between 1 and 10 was assigned to each configuration for each figure of merit, yielding a total score out of 10, with the optimal configuration having the highest score. To determine the weight and score of each component, research via trade studies and physical tests were performed. The configurations selected are outlined in green.

#### 3.4.1 Wing Position

Three possible wing position configurations were considered: low, middle, and high wing. The figures of merit considered were takeoff distance, ergonomics, stability, and maximum L/D. Ergonomics was defined as the aircraft's ability to store the electronics package and ease of access to it. Takeoff distance and ergonomics were weighted more heavily due to the 60 ft takeoff requirement and the 5 minute assembly time. The low wing was

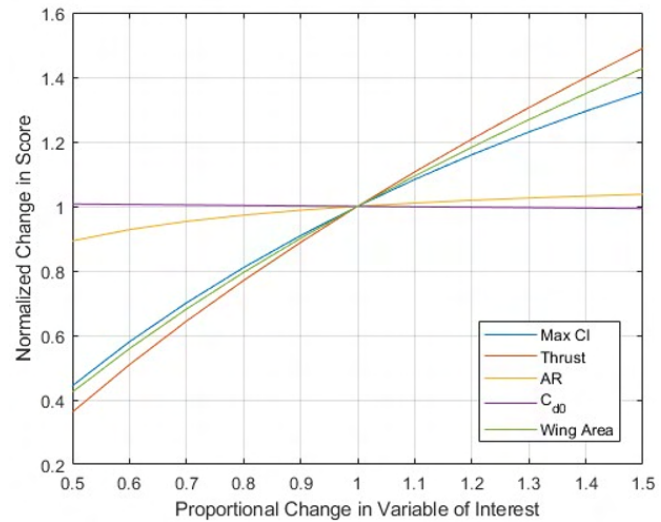


Figure 5: Score Sensitivity

selected due to the benefit of permitting a top access hatch, which would be more challenging to implement with the other configurations, requiring structure through the middle of the electronics package. While it had lower stability than the other two options, it performed better in regards to the challenge-specific requirements. The results are summarized below in Table 5.

Table 5: Wing Position Decision Matrix

<b>Figures of Merit</b>	<b>Factor</b>	<b>Low Wing</b>	<b>Mid Wing</b>	<b>High Wing</b>
Takeoff	0	Met	Met	Met
Ergonomics	0.4	10	6	8
Stability	0.4	7	8	8
Max L/D	0.2	8	9	9
	<b>Total</b>	<b>8.4</b>	<b>7.4</b>	<b>8.2</b>

### 3.4.2 Wing Shape

Four wing shapes were considered: straight, tapered, elliptical, and swept. The figures of merit were manufacturability, lift, stability, drag, box constraints, and ground mission compatibility. The GM criteria and high lift were prioritized to maximize M2 score. Manufacturability was prioritized next to allow for iteration and optimization of multiple wings. Box constraints and stability were equally weighted, since maximizing box dimensions would also lead to the most stable configuration by maximizing wing area and aspect ratio. Minimizing drag was also critical to improving performance; however, sensitivity analysis determined that reducing  $C_{D0}$  had a significantly lower effect on improving scores. Therefore, while the elliptical wing would have increased in-flight performance, its thin cross section and difficulty to manufacture made it disadvantageous, leading to a straight wing being the best choice.

Table 6: Wing Shape Decision Matrix

<b>Figures of Merit</b>	<b>Factor</b>	<b>Straight</b>	<b>Tapered</b>	<b>Elliptical</b>	<b>Swept</b>
Manufacturing	0.175	10	9	1	9
Lift	0.2	8	6	10	5
Stability	0.15	8	4	8	4
Drag	0.125	2	8	10	8
Box Constraints	0.15	8	6	10	7
Ground Mission	0.2	10	8	1	7
	<b>Total</b>	<b>8</b>	<b>6.875</b>	<b>6.325</b>	<b>6.625</b>

### 3.4.3 Tail Geometry

Six tail configurations were considered: conventional, cruciform, t-tail, v-tail, twin tail, and triple tail. The figures of merit considered were drag, weight, pitch stability, yaw stability, structural complexity, ease of manufacturing/ergonomics, and control complexity. Stability was considered the most important aspect, being the primary role of the tail. Analysis of the M3 antenna showed that its effect on yaw moments is more significant than pitching moments. Thus, priority was placed on yaw stability above all else. Control complexity considered control authority and implementation. Manufacturability and ergonomics took into account the difficulty of assembling the tail, which was highly valued due to all missions requiring an aircraft assembly time of less than 5 minutes. Low drag and weight were treated as lower priorities due to the tail's relatively small size compared to the rest of the aircraft. Structural complexity is the complexity of the structural elements required to construct the part to be rigid. Considering this, the conventional configuration achieved first place, with second place being the twin tail. The team ultimately decided on the conventional configuration for design simplicity and assembly time. The results are summarized in Table 7.

Table 7: Tail Geometry Decision Matrix

Figures of Merit	Factor	Conventional	Cruciform	T-Tail	V-Tail	Twin Tail	Triple Tail
Low Drag	0.1	7	7	9	10	5	3
Low Weight	0.1	9	9	9	10	7	5
Pitch Stability	0.2	8	7	6	6	8	8
Yaw Stability	0.25	8	5	5	6	9	10
Strength	0.1	8	6	5	8	8	8
Manufacturability/Ergonomics	0.15	9	6	6	7	8	6
Control Complexity	0.1	8	8	8	7	6	6
Total		8.15	6.55	6.45	7.25	7.65	7.2

### 3.4.4 Propulsion Configuration

The configuration of motors and batteries were the foci of propulsion conceptual design. Based on prior competition experience, single-tractor and twin-tractor motor configurations were considered in a figure of merit analysis. Higher motor numbers and pusher configurations were excluded due to their difficult integration and complex design. Maximum thrust, efficiency, and simplicity of design were factored equally highly, since their impact on aircraft design and total mission score were considered equal. Flight characteristic was defined as the influence on aircraft flight behaviors by the propulsion system, such as torque roll and prop wash. This was considered the second most important based on the philosophy of reducing mission difficulty for the pilot. Thrust-to-weight was assigned last, because its performance impact was considered the least substantial. According to the results depicted in Table 8, the single-tractor design was selected. Importantly, the implementation of the twin-tractor was found to severely compromise wing structures, wing area, and fitting into the box, and hence was scored

2 in simplicity of design. LiPo batteries were selected as the propulsion battery formula due to their superior

Table 8: Motor Configuration Decision Matrix

Figures of Merit	Factor	Single-Tractor	Twin-Tractor
Maximum Thrust	0.25	7	10
Efficiency	0.25	10	7
Simplicity of Design	0.25	10	2
Flight Characteristic	0.15	6	10
Thrust-to-Weight	0.1	10	6
Total		8.65	6.85

energy density, life span, and discharge rate over other alternatives. In addition, higher capacity battery cells were found to have higher efficiency and power-to-weight ratio when specific discharge rate (C-rating) is constant, with increased propulsion performance outweighing aircraft weight increase. Single-pack batteries were chosen over multiple smaller batteries for design simplicity and wiring weight reduction. Therefore, the decision was made to use single-pack batteries as close to 100 Watt-hours capacity as possible.

### 3.4.5 Landing Gear Selection

Four landing gear configurations were considered: wing taildragger, bow taildragger, strut tricycle, and bow tricycle. The figures of merit considered were drag, stability, takeoff speed, strength, and weight. Strength and takeoff speed were weighted the highest because of the M2 requirements for carrying the fully-loaded aircraft and lifting off within 60 ft. Weight was prioritized next because a lightweight design would improve the score for the GM and improve flight performance in general. Drag was considered for its substantial impact on the maximum speed of the aircraft, and stability was considered because the aircraft must remain maneuverable on the ground. The bow taildragger configuration was selected for its superior strength-to-weight ratio and for the increased takeoff speed with a greater angle of attack on the runway compared to the other configurations.

Table 9: Landing Gear Configuration Decision Matrix

Figures of Merit	Factor	Wing Taildragger	Bow Taildragger	Strut Tricycle	Bow Tricycle
Drag	0.1	8	8	7	7
Stability	0.1	7	6	8	8
Takeoff Speed	0.3	8	8	7	7
Strength	0.3	5	7	5	6
Weight	0.2	8	8	7	7
Total		7.0	7.5	6.5	6.8

## 3.5 Final Conceptual Design Configuration

The final *UW-23 Sailfin* configuration is a low-wing, single-engine, taildragger aircraft. It features straight wings with a downward twist and high aspect ratio. The wingtips feature adapters to accommodate a 39 in antenna

and a counterweight on the opposite side to mitigate roll tendencies introduced by the antenna. It is designed to carry a 9.33-lb electronics package and can sustain a 200-lb GM load.

## 4 Preliminary Design

Once configuration trade studies were completed, the HuskyWorks team began analyzing the selected configuration. The team used a combination of analysis and testing, with an iterative design process, to complete the preliminary design. This phase included conducting trade studies, building and breaking test components, and analyzing data. The results of preliminary design were used in making final decisions during detailed design.

## 4.1 Design Methodology

The design and analysis methodology used was built on the experience from prior competition cycles and advice from mentors. First, a sensitivity analysis was conducted using MATLAB R2022b [2]. Subsequently, different configurations were modeled using Open Vehicle Sketchpad (OpenVSP) [3] and the propulsion estimation tool eCalc [4]. These design concepts were weighed against each other and narrowed down into our preliminary configuration. This configuration was modeled and analysed using OpenVSP [3] and SolidWorks 2022 [5]. This analysis provided first estimates on expected aircraft performance, allowing for an aerodynamic prototype to be built to validate the design. Further detailed analysis was performed in XFLR5 [6] and AVL [7]. Performance analysis of the prototype led to further design iterations to produce an aircraft with better performance, manufacturing tolerances, and ergonomics. As shown in Fig. 6, iteration and verification is central to the design process, where each component is cyclically analyzed, improved, and validated to ensure high performance.

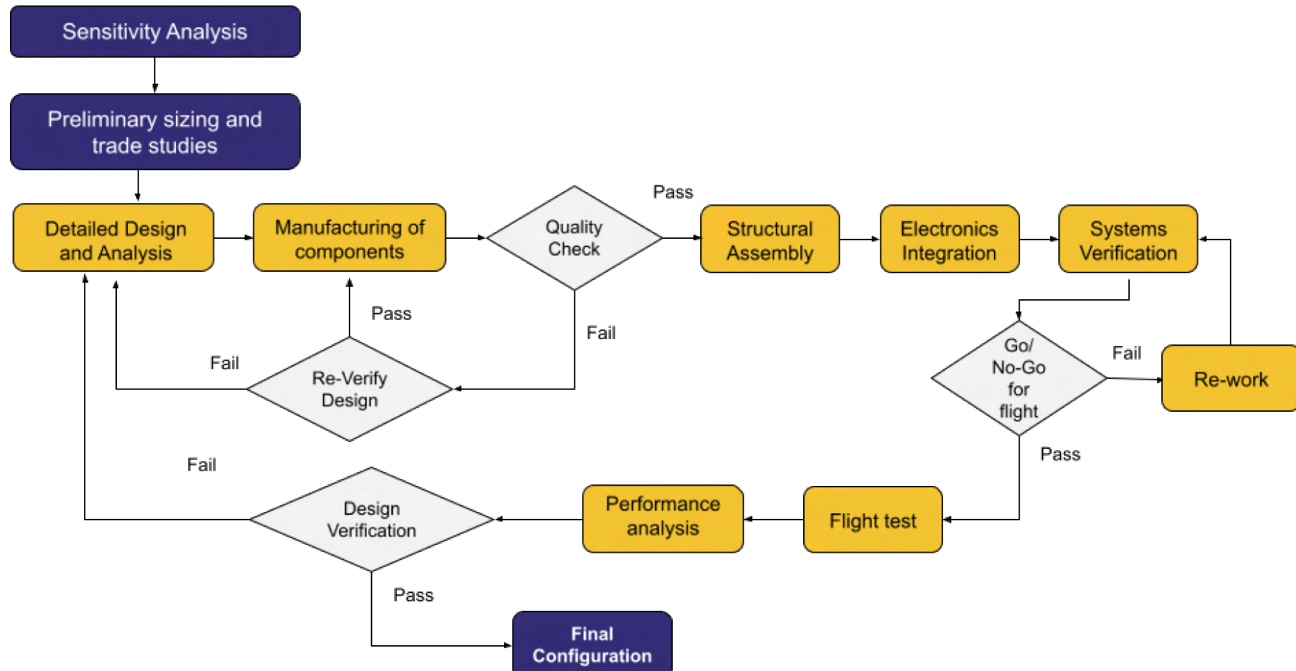


Figure 6: Design Methodology Flow Chart

## 4.2 Design and Sizing Trade Studies

### 4.2.1 Fuselage and Empennage Design and Sizing

The fuselage size was primarily dependent on the payload's dimensions. Competition requirements dictated the need for teams to carry a payload with minimum dimensions of 3.00 in x 3.00 in x 6.00 in. As a smaller cross section helps to minimize drag and empty weight, it was decided that the M2 payload would have the minimum possible dimensions, while the weight would be changed by drilling holes into the selected payload material. As the only other components required to be stored internally were the propulsion system, avionics system, and structural mounts, the cross sectional area was only constrained by the M2 payload and mount. The cross sectional shape was selected to be a filleted rectangle, as this had minimal impact on drag compared to a circle, was easier to manufacture and interface with other aircraft components, and best fit the cuboid payload. In addition to this, the fuselage was shaped such that the bottom would have no upward taper, while the top would taper upwards from the nose, and downwards towards the tail in a streamlined fashion. Because this year's aircraft is a taildragger configuration, tapering the lower fuselage upward would induce an undesirable greater angle of attack prior to takeoff rotation. In order to maximize the distance between the aerodynamic center of the wing and tail for better aircraft stability, the total length of the fuselage was determined to be 58 in. The side view of space allocation inside the fuselage is shown in Fig. 7.

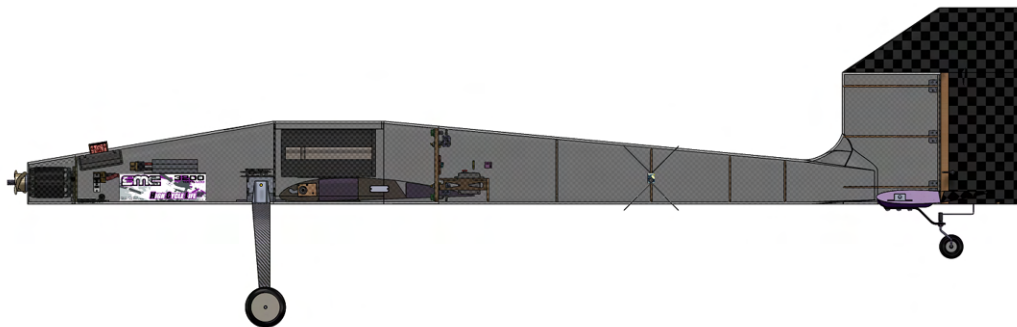


Figure 7: Fuselage Internal Space Allocation

The fuselage sub-team investigated semi-monocoque, monocoque and geodesic structures. A decision matrix was created, ranking accessibility and ergonomics highest, followed by weight, rigidity, ease of manufacturing, and cost. Accessibility and ergonomics were ranked highest because the aircraft assembly and payload installation must be completed within 5 minutes. Weight was ranked next, as the GM score is normalized by aircraft weight, and a lower weight will increase aircraft efficiency. Rigidity was ranked third because the deformation of the aircraft directly affects GM performance. Ease of manufacturing and cost were considered, but given the team's budget and experience with composites, they were ranked lowest. Although the geodesic frame had more room in the fuselage and a clear path to manufacturing, it would restrict the materials that could be used, increase weight, and have lower stiffness than the other options. A semi-monocoque fuselage was rigid and manufacturable, but when comparing weight and ergonomics, a monocoque fuselage was superior. Table 10

details these results.

Table 10: Fuselage Decision Making Matrix

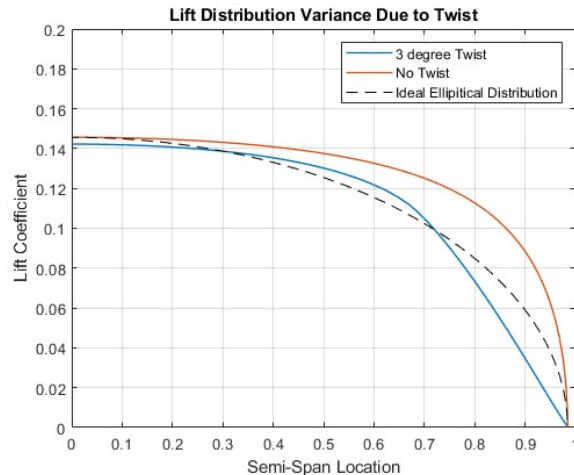
Figures of Merit	Factor	Carbon Fiber Monocoque	Carbon Fiber Semi-Monocoque	PLA Geodesic	Covering Film and Balsa Ribs
Accessibility/Ergonomics	0.26	7	3	9	8
Weight	0.24	9	6	1	6
Rigidity	0.22	8	7	5	1
Manufacturability	0.18	2	5	8	6
Cost	0.1	3	4	9	10
Total		6.4	5.06	6.02	5.82

#### 4.2.1.1 Wing Design & Sizing

The chord length and half of the wingspan were set to the interior dimensions of the box (38 in x 12.5 in) to maximize wing area while also maximizing the aspect ratio to 6.2. A higher aspect ratio was determined to be beneficial, as it decreases induced drag for M2 caused by the higher lift coefficient required to carry the payload. These dimensions were based on optimizing the length of antenna that could fit inside the box while still ensuring that the box had enough depth to contain the 4 wing sections and fuselage. Additionally, having a longer box allows for a longer fuselage, decreasing the size of the tail surfaces. The geometric twist of  $-3^\circ$  was determined to be the most effective angle of twist for the wing, per [8].  $-3^\circ$  gives a good approximation of an elliptical lift distribution, which further decreases induced drag. While the ideal wing twist to approximate an elliptical lift distribution was calculated to be  $-2^\circ$ , the wing twist implemented was increased to provide a larger margin for preventing tip stalls, increasing aileron authority in turns, and improving stall recovery, thereby allowing for tighter turns. The modified lift span distribution is shown in Fig. 8.

#### 4.2.1.2 Airfoil Selection

Airfoil selection was dependent on two factors: the need for high initial lift for the maximum takeoff weight within 60 ft (M2), and having the least drag for maximum speed (M3). While higher-lift devices other than simple flaps could be used to find the ideal balance, these were deemed unnecessary and too difficult to manufacture. The criteria developed, therefore, were divided into three categories in order of importance: takeoff, build characteristics, and maximum speed. These were further subdivided into  $C_L$  at an angle of attack of  $0^\circ$ , lift curve slope, stall angles of attack,  $\frac{C_L}{C_D}$  at takeoff angle of attack, sizing and ergonomics of the airfoil, manufacturability, and

Figure 8: Lift Distribution Benefit of  $-3^\circ$  Twist

$C_D$  at cruise angle of attack for maximum speed. These airfoils were evaluated at a Reynolds number of 525,000 for M1 and M2, and 825,000 for M3. Given these constraints, six potential airfoils were selected: NACA 2412, RAF 38, NACA CYH, NACA 4415, Clark Y, and S7055. Of the airfoils shown in Table 11, the Clark Y, S7055, and NACA 4415 stood out for high  $CL$  at  $0^\circ$  angle of attack, high  $\frac{C_L}{C_D}$  at takeoff angle of attack, high stall angle of attack, and simple manufacturing geometry. Of these, the Clark Y had the best blend of takeoff performance with the initial  $C_L$  and  $\frac{C_L}{C_D}$  with simple geometry.

Table 11: Airfoil Selection Decision Matrix

Figures of Merit	Factor	NACA 2412	RAF 38	NACA CYH	NACA 4415	Clark Y	S7055
$C_L @ A = 0$	0.15	8	8	8	9	9	9
$C_L vs A$	0.2	9	9	8	9	9	7
$C_D vs A$	0.1	7	7	6	7	8	7
$C_l/C_d vs A$	0.15	6	6	8	8	9	9
Ergonomics	0.2	8	7	6	6	8	8
Manufacturing	0.2	9	7	6	8	9	8
Total		7.8	7.3	7.0	7.8	8.7	8.0

#### 4.2.1.3 Tail Design & Sizing

In sizing the vertical and horizontal stabilizers, volume coefficients of 0.07 and 0.7, respectively, were chosen, consistent with historical data from Raymer [8] for general aviation aircraft, and slightly over sizing the vertical stabilizer to counteract antenna yaw. Surface area was determined using wing reference area ( $968.75 \text{ in}^2$ ), wingspan (77.5 in), wing aerodynamic chord (12.5 in), and wing-to-tail ac-to-ac distance (37 in). To maximize the  $C_L vs \alpha$  slope, the vertical tail has no sweep angle. Box size limited the largest stabilizer dimension to 12.5 in. For the vertical tail, the resulting dimensions were 12.5 in of height, and 11.36 in at maximum chord, producing  $142.04 \text{ in}^2$  of area. The corresponding dimensions for the horizontal tail were 30.7 in of span and 7.45 in of chord. After noticing undesirable aeroelastic effects during a test flight due to the oversized rudder notch, a leading edge taper was introduced starting at 8.33 in height and maximum chord to full height and 45% chord (shown in Fig. 9), resulting in a decrease of 10% of tail area and a new vertical tail volume coefficient of 0.0636.

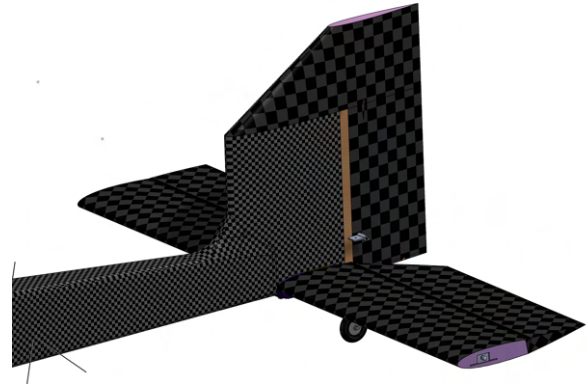


Figure 9: Tail Configuration

#### 4.2.1.4 Control Surface Sizing

Four primary control surface types were defined for the *Sailfin*: elevators, rudders, ailerons, and flaps. Historical data, current research papers for similar class aircraft, and mission constraints guided sizing. From this information, the elevator was eventually determined to span the entire horizontal stabilizer, and take up 45% of the chord. To counteract the yaw moment introduced by the antenna, the rudder was oversized, and included a notched aerodynamic balance. The bottom 8.33 in of the rudder spans 45% of the vertical stabilizer chord, and the notch spans the full chord length with a leading edge taper. Approximate  $C_L$  vs deflection angle plots generated (see Fig. 10) using Python scripts and XFOIL [9] data, were used to examine the lift power of the rudder at various deflection angles and its ability to counteract the yaw moment induced by the antenna. The ailerons span 50% of the wingspan and 33% of the chord, while the flaps span 50% of the wingspan and 33% of the chord.

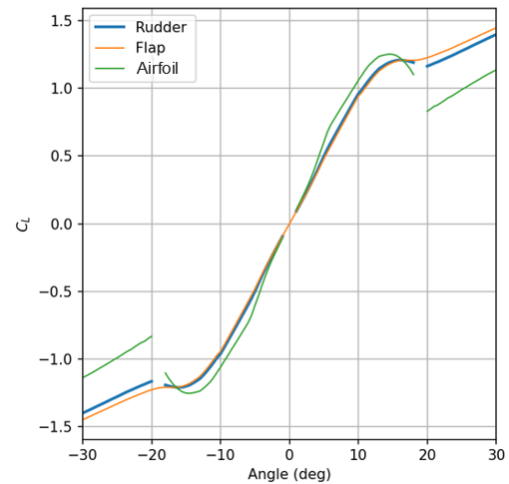


Figure 10: Increase in  $C_L$  vs Control Surface Deflection

#### 4.2.2 Avionics and Propulsion Design and Sizing

##### 4.2.2.1 Propulsion Design & Sizing

The goal of propulsion design was to provide maximum thrust under the power limit determined by flight time and battery capacity. To determine the power limit, the relationship between average propulsion power, energy loss due to heat, and total battery capacity was modeled using Equation 6.

$$P_{prop} \cdot t_{est} + P_{loss} \cdot t_{est} = E_{batt} \text{ where } P_{prop} = V \cdot I \text{ and } P_{loss} = I^2 \cdot R_{sys} \quad (6)$$

Observing the equation, it was deduced that increased voltage at the same electrical power would reduce energy loss due to decreased current. Therefore, the largest FAA and DBF compliant 6S and 8S batteries were considered in the analysis, with higher cell-count batteries excluded due to lack of availability. Using an estimated total flight time of 10.5 minutes and 1.75 minutes for M2 and M3 respectively, the average propulsion power limit was calculated for each battery, with burst current restricted to under 100 A permitted by the fuse.

Table 12: Battery Decision Matrix

Configuration	Total Capacity (Watt-hour)	M2 Average Power (Watt)	M3 Average Power (Watt)	Takeoff Power Limit (Watt)
6S 4500 mAh	99.90	520.7	2220.0	2220.0
8S 3200 mAh	94.72	506.9	2451.7	2960.0

Following the results of Table 12, the 8S 3200 mAh battery was chosen for its better overall performance with a small disadvantage in M2 power limit. Furthermore, a minimum rating of 35C was specified for the 8S 3200

mAh batteries to allow safe discharge up to 100A. Lastly, with the team's sponsorship by SMC, the SMC 8S 3200mAh 75C LiPo batteries were selected as the preliminary propulsion battery pack. Subsequently, various propulsion systems were evaluated at the determined power limits using manufacturers' data sheets. Due to the team's partnership with T-Motor, only T-Motor brushless outrunner motors were considered in the analysis. The motors were evaluated on the same propeller for a direct comparison in their ability to produce torque and RPM. Eventually, the T-Motor AT4140 410KV motor was selected for its superior thrust performance under all power limits and its headroom to accommodate higher-loading propellers if necessary. In combination, the APC 16X12E and 17X10E propellers were chosen based on preliminary aerodynamic design. Finally, the APD 120A F3[X] was selected as the ESC for the AT4140 due to their zero-failure record with the team last year, large factor of safety, and telemetry capability assisting performance analysis. Overall, the preliminary propulsion system is summarized by Table 13.

Table 13: Preliminary Propulsion Design

Motor	ESC	Propulsion Battery	Propeller Choice	
T-Motor AT4140 410KV	APD 120A F3[X]	SMC HCL-HVP 8S 3200mAh 75C	APC 16X12E	APC17X10E

#### 4.2.2.2 Avionics Design & Sizing

The focus of the preliminary avionics design was sizing the actuators of flight control surfaces to guarantee controlled flight. Given the required hinge moments for each control surface, it was concluded that 4.34–5.21 lb·in of torque was required for each elevator, flap, and aileron surface, and 15.62–20.83 lb·in of torque was required for the rudder. After analyzing the torque to weight ratios of multiple servos that satisfy the torque demand, servos were selected from KST, a sponsor of the team. Based on manufacturer specifications, the KST X15-1809 servo was selected for the rudder, and the KST X10 Mini servo was selected for all other control surfaces.

### 4.3 Aircraft Stability Analysis

#### 4.3.1 Static Stability

To ensure the aircraft was statically stable in all flight regimes, the CG of the aircraft was set to be within  $\pm 0.1$  chord lengths of the aerodynamic center of the aircraft during level flight in all missions. The electronics package mounting location was chosen such that its CG was coincident with the aircraft's CG, to minimize changes between flights. The CG was determined to be at the 0.34, 0.30, and 0.33 chord points of the wing for M1, M2, and M3, respectively. The neutral point was determined to be located at the 0.561 chord point from the model created in XFLR5 [6]. This produces a static margin of 22.5%, 26%, and 23.42%. The static margins are greater than the typical static margin for an aircraft of this configuration to counter the increased pitching moment generated by the antenna. The aircraft's stability derivatives were calculated in AVL [7] and are displayed in Table 14. All values possess the correct signs to indicate stable flight behavior. This analysis was only performed for

M1 and M2 due to deficits in stability analysis programs' abilities to model asymmetric configurations accurately.

Table 14: Stability and Control Derivatives for M1 and M2

Mission	Stability Derivatives [rad^-1]			Control Derivatives		
	$dC_l/d\beta$	$dC_m/d\alpha$	$dC_n/d\delta\beta$	$dC_l/d\delta f$	$dC_m/d\delta a$	$dC_n/d\delta e$
M1	-0.022	-0.969	0.092	0.023	0	0.022
M2	-0.036	-0.976	0.096	0.023	0	0.022

For setting the angle of incidence of the wing, the wing's coefficient of lift was determined to be sufficient at zero angle of incidence for M1 and M3, operating at the minimum drag condition for the aircraft to maximize speed in M3. The  $C_M$  was found to be 0 for M3, while producing a trimmable stable flight condition for M1 and M2, despite the excess downward pitching moment, as shown in Fig. 11d.

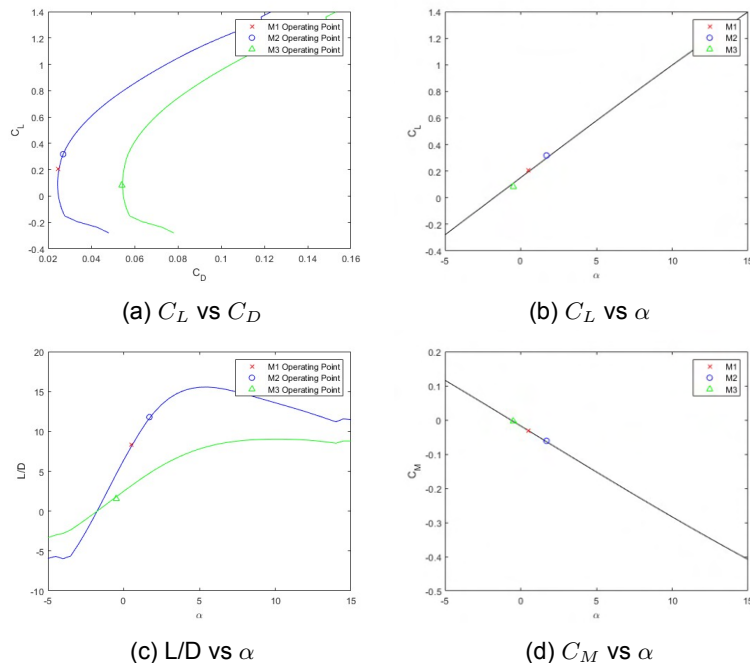


Figure 11: Aircraft Performance Curves

### 4.3.2 Dynamic Stability

To verify the aircraft's dynamic stability, the program XFLR5 [6] was used to determine all of the eigenmodes of the aircraft. These eigenmodes were then imported into MATLAB [2] to generate Fig. 12. All 5 of the eigenmodes have negative real values, meaning that the aircraft is dynamically stable for all lateral and longitudinal eigenmodes. For the dissipation of perturbations, the greatest time to halve for all 3 mis-

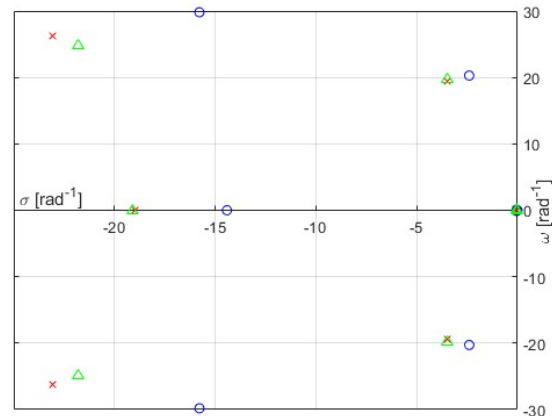


Figure 12: Root Locus Plot for all Eigenmodes

sions for the short period longitudinal mode, the dutch roll mode, and roll mode are 0.044 s, 0.297 s, and 0.050 s, respectively. These modes naturally dampen out without the need for pilot correction. However, the phugoid and spiral modes have very small damping properties, with times to halve greater than 20 s for the phugoid mode and 80 s for the spiral mode. Both the spiral and phugoid modes will require some pilot assistance in flight to compensate.

## 4.4 Aircraft Performance Analysis

A variety of hand calculations and computational methods were involved in characterizing this year's aircraft performance. Both inviscid and viscous CFD simulations, OpenVSP [3] analysis functions, and traditional performance equations obtained from Anderson [10] were used. Due to the asymmetric nature of the M3 configuration, correctly predicting performance required this layered approach.

### 4.4.1 Drag Analysis

To compute the total drag of a proposed aircraft design, there are several different tools that are capable of determining the drag of an aircraft using inviscid techniques for a conventional aircraft design. However, due to the presence of the  $\frac{1}{2}$  in PVC pipe, inviscid analysis would generally fail due to the flow separation guaranteed behind the pipe. Therefore, the drag of the antenna needed to be calculated separately from the inviscid solution used on the main aircraft.

#### 4.4.1.1 Antenna Drag

Initial analysis of the antenna was done using the well-documented drag coefficients of a cylinder in a uniform flow. Using the projected Reynolds numbers of 50,000-65,000 gives a drag coefficient of 1 for the diameter. Using the general drag equation (Eq. 7), where  $A_l$  is the antenna length yields a drag of 4.225 lb at 131 ft/s.

$$D = C_d \cdot q \cdot d \cdot A_l \quad (7)$$

Several CFD estimates were used to attempt to model the antenna's actual drag, but due to the turbulent and viscous nature of the flow behind the antenna, these methods were not able to accurately characterize this flow at high Reynolds numbers. All drag values produced from Ansys Fluent [11] underestimated the drag produced by the antenna, with typical results being 2.25 lb of drag, nearly a factor of 2 less than what was initially calculated. Therefore, the greatest possible drag value was used to compensate for any underestimates that would otherwise compromise the aircraft's stability.

#### 4.4.1.2 Aircraft Drag

The lift and drag characteristics of the *Sailfin* were evaluated using OpenVSP. The OpenVSP parasitic drag solver uses linear inviscid models to calculate the parasitic drag coefficient of each individual component and sums them together. The induced drag was calculated from the required  $C_L$  for each mission and from the induced drag formula shown in Eq. 8. Due to the inviscid nature of OpenVSP, the results are not accurate at high angles of attack due to flow separation. These results were then combined into Fig. 13 which shows the

drag of each individual aircraft component for each mission. The antenna's drag was added for M3 from the separate calculation.

$$C_{di} = \frac{1}{\pi \cdot e \cdot AR} \cdot C_l^2 \quad (8)$$

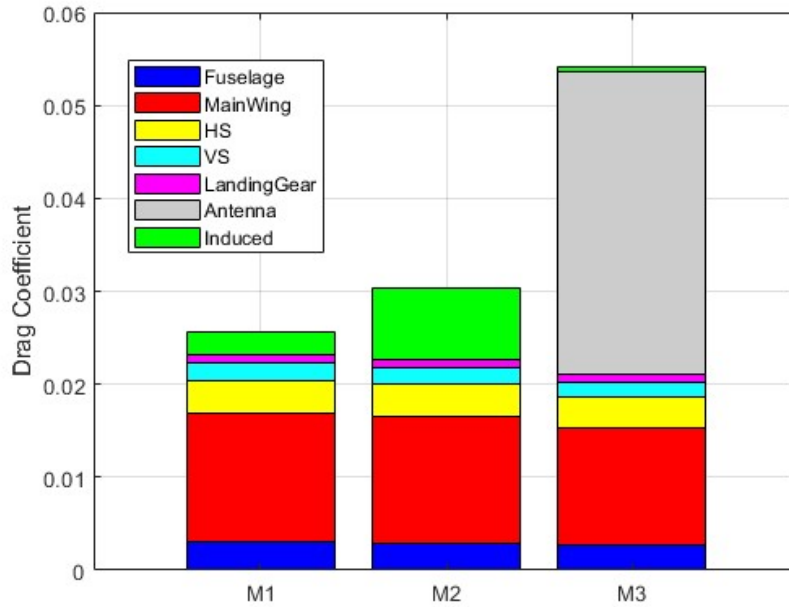


Figure 13: Mission-Specific Drag Breakdown

From Fig. 13, the greatest source of drag on the aircraft comes from the wetted area of the wing across all 3 missions. However, during M3, the greatest source of drag is the antenna. The added drag during M3 contributes to a lower L/D for the mission due to the increased drag of the antenna, but lower required lift from the greater cruise speed. This is acceptable due to the non-standard drag conditions for the antenna, as the higher drag will tend to decrease L/D.

#### 4.4.2 Takeoff Distance

Analysis was performed to determine the effect of takeoff weight on takeoff distance. The takeoff distance is proportional to the square of takeoff weight, as shown in Eq. 9, obtained from Anderson's Introduction to Flight [10]. This results in a theoretical maximum takeoff weight of just over 23.5 lb for the aircraft within the required 60 ft takeoff distance. The weight was determined using standard atmosphere at 2500 ft and full throttle, and these conditions were used for all further takeoff distance calculations. Increased weight impacts other characteristics of the aircraft, especially handling.

$$s_{LO} = \frac{1.44W^2}{g\rho_\infty SC_{L,max}\{T - [D + \mu_r(W - L)]_{av}\}} \quad (9)$$

While 23.5 lb was the maximum possible takeoff weight for the aircraft, based on the M2 analysis done, the optimum payload weight for the mission was 9.33 lb, which yields an approximate total weight of 18.33 lb based on material and electronic weight estimations. The estimated takeoff distance at this weight is 41.5 ft, providing sufficient margin for a variety of flight conditions, while optimizing M2 score. Shown below in Fig. 14 is a plot comparing aircraft weight to takeoff distance, with the magenta line representing the 60 ft takeoff distance limit. All 3 mission weights are plotted and labeled. All vertical lines intersect the takeoff distance curve below the magenta line, verifying that the aircraft can meet the takeoff requirement for all missions.

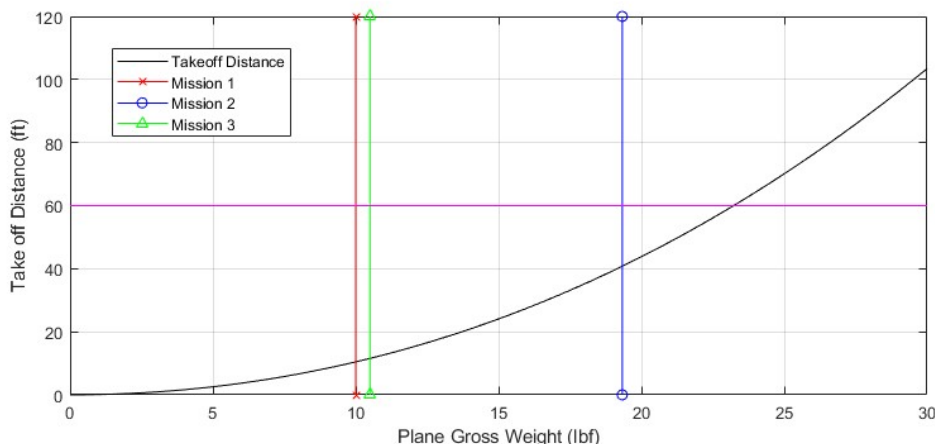


Figure 14: Takeoff Distance for M1, M2, and M3

#### 4.4.3 Turning Radius

Several ideas, including slotted flaps, vortex generators, leading edge slats, and slotted airfoils were evaluated as potential methods of increasing the aircraft's ability to bank at both maximum speed and minimum turn radius. However, after exploring the different options and constraints, it was determined that implementing the favored devices, slotted flaps, would lead to an increase in weight and manufacturing complexity that would outweigh potential improvements in turn performance. Therefore, traditional control surfaces alone were implemented as the aircraft's turning mechanisms. The maximum structural loading for the aircraft was determined to be 4g, which allows for a 75° maximum bank angle. Using this and the level turning radius equation shown in Eq. 10, a plot of turning radius vs cruise speed was generated, shown in Fig. 15. The solid lines show the turning radius, assuming constant speed and increasing thrust during the turn to match the increase in induced drag. The dashed lines show the turning radius based on constant thrust and the decreased velocity due to the increased induced drag. As all of the constant thrust speeds are above stall speed, there is no concern of the aircraft stalling in the turn at the selected bank angle.

$$R = \frac{v^2}{g \cdot \tan \theta} = \frac{v^2}{g \cdot \sqrt{n^2 - 1}} \quad (10)$$

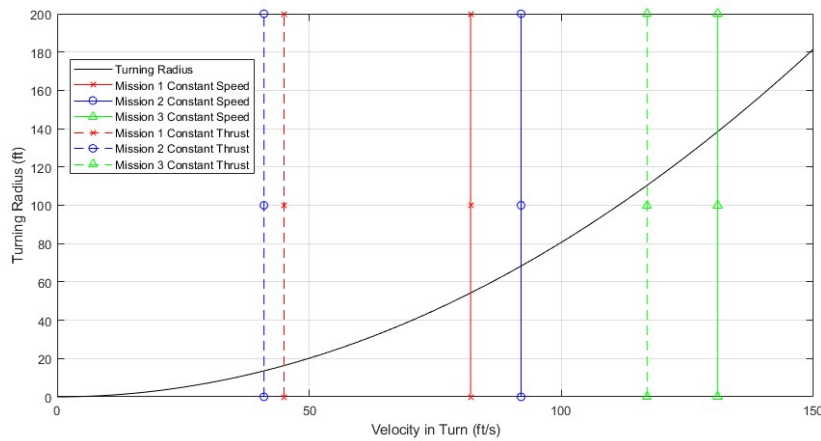


Figure 15: 4g Turning Radius for Constant Speed and Thrust

#### 4.4.4 Power Curve

Two propellers, the APC 16X12E and 17X10E, were chosen to overcome aerodynamic drag and achieve optimum speeds in each mission. After total drag was calculated from OpenVSP's drag analysis functions, propeller models were created for performance at designed mission flight speeds in conjunction with RPM. Data from APC's performance database was then tabulated with respect to flight speed and motor RPM. Because M2 required higher thrust to carry the weight of the electronics package, it was deemed necessary to use a prop with higher pitch, unlike the other missions. In the case of M3, its higher top-speed drag, generated by the antenna, meant that compared to M1, the motor would have to operate at a higher RPM for the same speed. The two models shown in Fig. 10 illustrate the performance of the selected props, where the 17X10E corresponds to M2 and the 16X12E corresponds to M1 and M3.

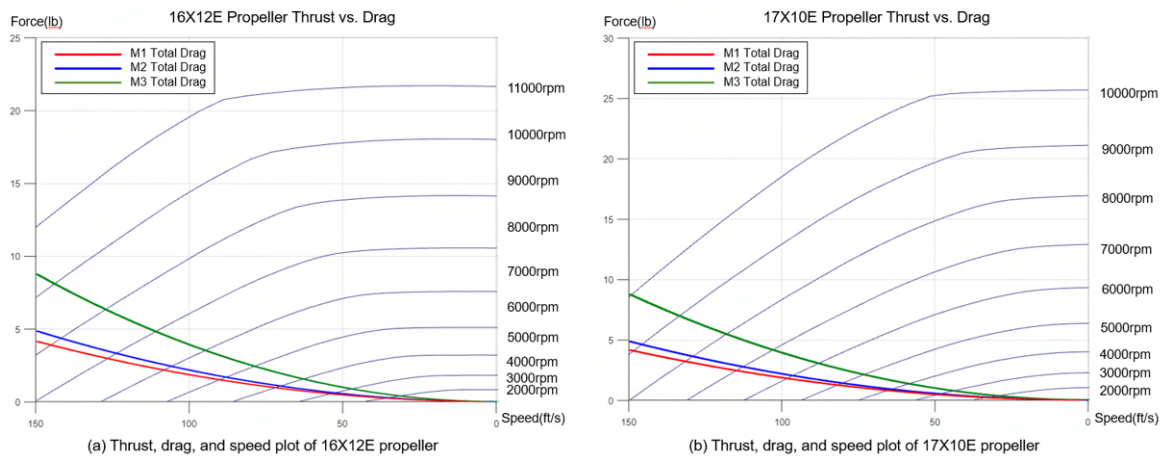


Figure 16: Thrust, Drag, and Speed Plots for (a) 16X12E Propeller and (b) 17X10E Propeller

#### 4.4.5 Endurance

Due to the 100 Wh battery restriction, the endurance for each mission was estimated based on calculated drag values. The required power for each mission was calculated by multiplying drag by velocity to produce the average power required for the mission. The total efficiency of the propulsion system is a function of velocity and RPM, producing maximum total usable energy of the battery at 87Wh. The power required was computed using Eq. 11, and the total flight time was found by dividing the usable energy by the power required. This produces an endurance of 8.8 minutes for M1, 10 minutes for M2, and 4.5 minutes for M3. All listed endurance values exceed mission requirements and provide enough buffer for takeoff and landing.

$$P = C_d \cdot q \cdot S \cdot V \quad (11)$$

### 4.5 Environmental Uncertainties

Due to using an array of performance-characterizing methodologies with different assumptions, the accuracy of results relative to their expected real-world values was reduced. Therefore, it was necessary to consider the effects of real-world environmental conditions to build a margin of error into the aircraft's performance, such that it could perform similarly in both flight tests and the actual competition. The conditions expected in Tucson, in addition to the conditions in which the aircraft was tested are listed below in Table 15. Instead of using standard day conditions for the analysis given what is known about the competition location, a set of 10% hot day conditions at 2500 ft for our analytical baseline worst-case was adopted, based on MIL-HDBK-310. Calculations were performed assuming winds will be less than 10 knots gusting to 25 knots for outlier case evaluation, otherwise still wind conditions are assumed. Based on the team's previous experience with wind gusts in Wichita, the effects of wind gusts greater in magnitude than those in the team's hometown of Seattle were considered. This was accounted for by ensuring that margins were built into stall speed calculations and avoiding flight at maximum thrust, to provide extra thrust in the case of rapid flight condition changes. The temperature was set to 87° F for all simulations to better represent the conditions at the competition site. This increase in temperature was also assumed to lead to an improvement in battery performance.

Table 15: Comparison of Testing Location vs. Competition Location Conditions

Uncertainty	MMRC Park, Redmond, WA	TIMPA, Tucson, AZ
Season	Winter	Spring
Average High Temperature (°F)	47	87
Average Wind Speed (mph)	11.4	12.5
Environment Type	Mountainous Temperate Oceanic	Intermediate Desert Plain
Afternoon Humidity	74%	24%
Airfield Elevation (ft)	43	2389

## 4.6 Predicted Aircraft Mission Performance

Shown in Table 16 are the relevant aircraft and mission performance values of interest for all flight missions. For M2, the aircraft will carry 9.33 lb of payload, travel at 92 ft/s, and complete 13 laps inside the 10 minute flight window. The longer lap time for M2 stems from needing a smaller bank angle to prevent stall and structural damage. For M3, the aircraft will fly with a 39 in antenna and travel at 131 ft/s, with a total mission time of 1.45 minutes for the required 3 laps. The decreased L/D parameter on M3 comes from the decreased lift due to the increased cruise speed at which the aircraft travels, and the increased drag due the addition of the antenna.

Table 16: Predicted Mission Performance for M1, M2, and M3

Parameter	Mission 1	Mission 2	Mission 3
Weight (lb)	10.00	19.33	10.50
Wing Loading (lb/ft <sup>2</sup> )	1.49	2.87	1.56
Cruise $\alpha$ (deg)	0.50	1.70	-0.50
Cruise Lift Coefficient	0.205	0.318	0.084
Cruise Drag Coefficient	0.025	0.028	0.054
Cruise Lift-to-Drag Ratio	10.2	11.4	1.6
Cruise Airspeed (ft/s)	82	92	131
Stall Airspeed (ft/s)	31	37	31
Takeoff Ground Roll (ft)	10.5	40.8	11.6
Turn Radius (ft)	54.3	68.3	138.5
Endurance (min)	8.8	10.0	4.5
Lap Time (s)	32	43	29
Mission Time (min)	1.6	10.0	1.5

## 5 Detailed Design

The detailed design phase uses what was learned and selected during trade studies and preliminary design to optimize the aircraft. An analysis of previous competition scores showed that the aircraft that successfully completed all four competition missions often place within the top 20 teams, guiding the HuskyWorks team to focus on aircraft reliability and survivability. Subsystem design was iterated to reduce weight, increase efficiency, and improve reliability.

### 5.1 Dimensional Parameters

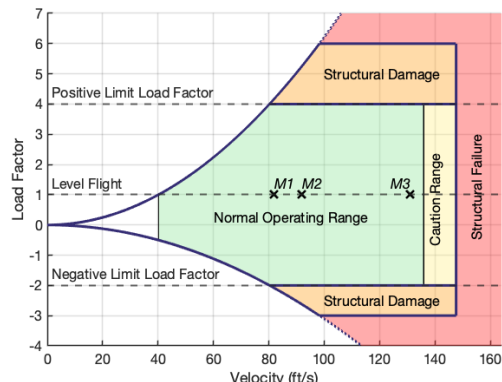
Table 17 shows the dimensions and components of each main subsystem in the aircraft.

Table 17: Sailfin Dimensions and Component Specifications

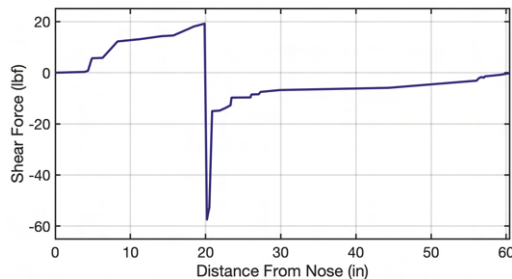
Wing		Horizontal Stabilizer		Propulsion	
Airfoil	Clark Y	Airfoil	NACA 0012	Motor Model	T-motor AT 4140
Span	77.5 in	Span	30.97 in	Motor Rated KV	410 KV
MAC	12.5 in	Chord	7.46 in	Motor Weight	1.23 lb
AR	6.2	AR	4.15	Propellers	APC 16X12E, APC 17X10E
Wing Area	968.75 in <sup>2</sup>	H-stab Area	231.04 in <sup>2</sup>	Propulsion Battery	SMC HCL-HVP 8S
Root Chord	12.5 in	Angle of Incidence	0 deg	Propulsion Battery Capacity	3200 mAh
Tip Chord	12.5 in	Fuselage			
Taper Ratio	1	Total Length	58 in	Max Discharge Rating	75C
Leading Edge Sweep	0 deg	Tapered Nose Section Length	14.43 in	Weight per Pack	1.61 lb
Angle of Incidence	0 deg	Straight Midsection Length	11.68 in	Model	APD 120A F3[X]
Static Margin (M1, M2, M3)	22.5%, 26%, 23.42%	Empennage Length	31.89 in	Rated Voltage	50.4 V
		Midsection Height	5.25 in	Continuous Current	120 A
Vertical Stabilizer		Midsection Width	3.5 in	Controls	
Airfoil	NACA 0012	Empennage Minimum Height	1.83 in	Transmitter	Radiomaster TX16s
Height	12.44 in	Empennage Minimum Width	1.30 in	Receiver	FrSky R-XSR 2.4GHz Micro
Root Chord	11.36 in			Avionics Battery	Lumenier 1300mAh 3S
Tip Chord	5.21 in	Normal Operating Range		Weight per Pack	0.216 lb
V-stab Area	128.68 in <sup>2</sup>	Nose Minimum Height	3.04 in	Wing Servos	KST X10 mini
AR	1.2	Nose Minimum Width	2.75 in	Rudder Servo	KST X15-1809
Leading Edge Sweep	0 deg	Corner Fillet Radius	0.5 in	Elevator Servos	KST X10 mini

## 5.2 Structure Characteristics and Capabilities

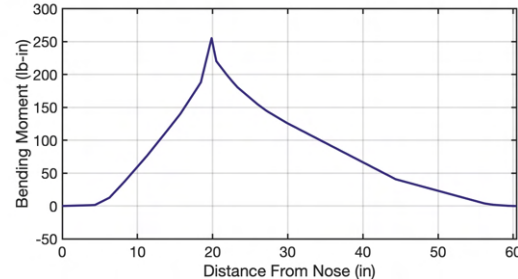
The structural design process for the *Sailfin* primarily focused on ensuring the aircraft could withstand the aerodynamic, inertial, propulsive, and ground forces encountered during each flight mission and GM. The aerodynamic loads primarily act on the wing and tail assemblies, while propulsive and inertial loads primarily act on the fuselage. The ground loads consist of the impact of the landing gear when touching down on the runway, as well as the shear forces and bending moment applied to the wing during GM. The structural design also takes into account the assembly time of the aircraft and the need for efficient and stable flight. Consideration was given to overall weight, center of gravity, and weight distribution. The *Sailfin*'s components were designed to withstand a load factor of 4g with a factor of safety of 1.5 in order to minimize weight while maintaining structural integrity and meeting mission performance expectations. In order to design the aircraft with the correct structural margins, the flight loads were estimated by analyzing corner cases of the V-n flight envelope shown in Fig. 17. The wing loading was determined from the lift distribution shown in Fig. 8 in Section 4. The fuselage loads for 4g turns were determined from the weight distribution of the aircraft and aerodynamic forces and moments acting on the body using the method outlined by Bruhn [12]. The most critical loading conditions associated with M2 are shown in Fig. 18.

Figure 17: *Sailfin* V-n Diagram

The aircraft was designed to withstand these shear forces and bending moments for a sustained duration while also providing the ability to exceed these loads for short bursts if needed.



(a) Estimated Shear Force in Fuselage During 4g Turn with M2 Payload



(b) Estimated Bending Moment in Fuselage During 4g Turn with M2 Payload

Figure 18: Critical Case Shear and Bending Moment Diagrams of Fuselage

## 5.3 Sub-system Design

### 5.3.1 Fuselage Design

The fuselage has a 58 in long carbon fiber monocoque body divided into three sections: a tapered nose, a rectangular fuselage, and a tapered empennage. The rectangular fuselage has a 3.5 in x 5.25 in rectangular cross section with 0.5 in fillets. This section was composed of a honeycomb core sandwiched between two layers of prepreg carbon fiber. A 3.5 in x 5.5 in access hatch was placed above the wing spar for payload access. The fuselage supports the electronics package and requires the integration of the wing mount, landing gear mount, and motor mount. The vertical stabilizer was built into the empennage. This section was manufactured in the same layup as the fuselage and nose, but was separated after curing for storage in the box. Both the nose and empennage were made of a prepreg carbon-honeycomb sandwich panel. When the aircraft is assembled out of the storage box, the empennage is connected to the fuselage by means of a locking pin mechanism attached to bulkheads on the aft end of the fuselage section and the forward end of the empennage. The monocoque structure of the fuselage allows for the skin to be the main load-bearing component. Seven bulkheads constructed of 1/8 in plywood were added along the length of the fuselage, empennage, and vertical stabilizer for alignment and support at critical interfaces, such as the joint between the empennage and the fuselage section.

### 5.3.2 Payload Storage Design

The payload storage system consists of the M2 electronics package and electronics package mount. In order to minimize fuselage cross-sectional dimensions, the electronics package was designed to be 3.00 in x 3.00 in x 6.00 in. It is comprised of a steel core and 3D printed exterior shell. The final payload weight was 9.33 lb as determined by the sensitivity analysis. The payload also has a canvas handle for ease of installation and removal.

The M2 payload mount was designed to hold the electronics package above the main wing spar in order to force the primary load through this spar. The mount was designed to create a

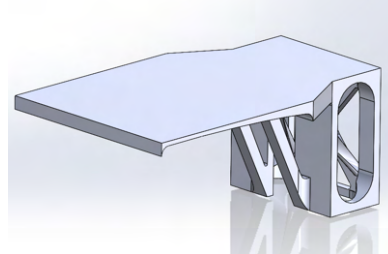


Figure 19: M2 Payload Mount

flat mounting surface over the curved wing spar. The mount was 3D printed in PETG plastic and optimized for weight. As shown in Fig. 19, a truss structure was used to allow wiring to pass through and for access to the wing mount. Reusable adhesive strips were added onto the mount to secure the payload while in flight.

### 5.3.3 Wing Design

The wing structure was designed for a 200 lb GM load and a maximum 4g turn during M2 flight. Based on prior experience and testing, a 200 lb load was deemed realistic without incurring severe weight penalties. The overall structure, shown in Fig. 20, consists of two wing segments connected by a center spar. The team designed and built the main wing spars, as well as the center spar, to withstand all flight and GM loads. The structure was analyzed using a pinned-pinned beam for the GM and cantilever beam for flight loads. The maximum loading case for all failure modes was the 200 lb GM load, thus the wing structure was designed with the goal of withstanding a point force of 200 lb directly in the center of the fuselage. Because of the boundary conditions, the maximum bending moment was at the center of the fuselage, thus the center spar was designed to be stronger than the main wing spars. The spar sandwich core material was kept constant across the wing, as the shear force was approximated as constant during GM. Three failure modes were identified prior to starting wing structural analysis: shear failure of the core, yielding of the skin, and buckling of the skin, which are detailed in the following subsections.

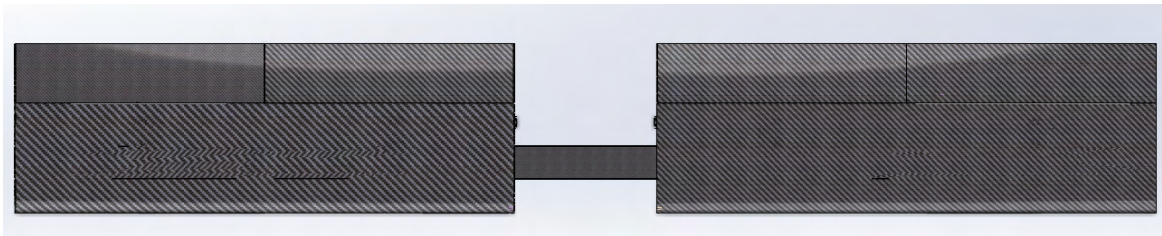


Figure 20: Top View of Wing

#### 5.3.3.1 Core Shear Failure

The maximum shear stress during GM and during flight were 76 psi and 53 psi, respectively; thus, shear failure was dominated by GM loading. An XPS foam core was initially selected, however, analysis determined that the foam alone could not take the shear stress. Two strips of 1/8 in balsa were added on the vertical sides of the spar to act as shear webs. The factor of safety for shear failure with the balsa and foam was calculated to be 1.8. Equation 12 was used to calculate the shear stress.

$$\tau = \frac{P \cdot Q}{t \cdot I} \quad (12)$$

Additionally, since the center spar and main wing spars are discontinuous, there was a concern of failure at this connection point, as there is no shear resistance. This was resolved by adding a small carbon fiber rod at the center of the spar at these connection points. Hand calculations determined that it needed to be 0.1 in in

diameter, thus a 0.24 in spar was selected as it was readily available to the team and did not add significant weight.

### 5.3.3.2 Yield Failure

The bending stress of a sandwich was calculated using Eq. 13, where  $M$  is the maximum moment,  $h$  is the distance between the center of the skins,  $t$  is the thickness of the skin, and  $b$  is the base of the beam. The maximum bending stress was calculated to be 43.6 ksi. When compared to the ultimate strength of carbon fiber, the factor of safety was well over the required margin at 10.

$$\sigma_b = \frac{M}{h \cdot t \cdot b} \quad (13)$$

### 5.3.3.3 Shear Crimping (Buckling)

The failure mode that determined the number of layers of unidirectional carbon fiber on the center spar was shear crimping. A MATLAB script [2] was developed to iterate the number of layers against the critical buckling load. Equation 14 was used to calculate the stress at which shear crimping would occur, where  $\sigma_{fw}$  is dependent only on the material properties of the core ( $G_c$  and  $E_c$ ) and carbon fiber ( $E_f$ ). The critical moment at this stress was calculated using Eq. 13, and the critical load was calculated from this moment. The critical load plotted against the number of layers is shown in Fig. 21. This plot shows that 4 layers of UD are required to resist shear crimping. To provide an additional factor of safety for a mission critical part, the team added an additional layer.

$$\sigma_{fw} = \frac{1}{2} \cdot (G_c \cdot E_c \cdot E_f)^{\frac{1}{3}} \quad (14)$$

Ultimately, the center and main wing spars have an XPS foam core with balsa shear webs, and unidirectional carbon fiber sandwiched on the top and bottom. The center spar has 5 layers on the top and bottom, while

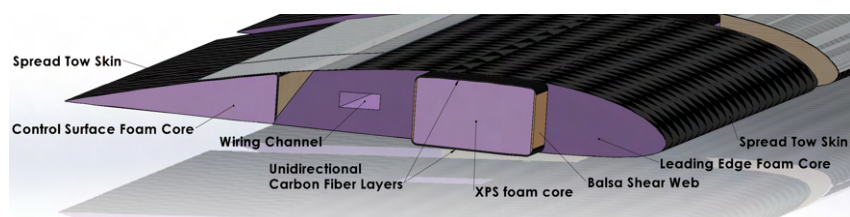


Figure 21: Wing Spar Analysis

the main wing spar has 2. The leading and trailing edges, as well as the control surface are XPS foam. The whole wing is wrapped in 45 degree spread tow to resist torsion and provide additional stiffness.

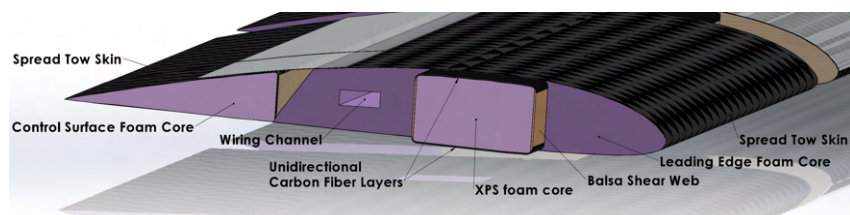


Figure 22: Wing Section View

### 5.3.4 Wing Mount

The primary wing mount serves as the loading point for the M2 payload as well as the main attachment between the wing and fuselage. As shown in Fig. 23, the mount follows the shape of the wing spar to allow for maximum contact between the spar and mount, distributing load. It was determined that the weakest point of the mount is the epoxy bond between the mount and the fuselage. Hand calculations were performed to determine the thickness of the flange needed for the glue to withstand a tensile force due to the ground mission load, as well as high g turns. To lock the wing in place, a low-profile off-the-shelf latch, placed flat against the side of the fuselage, was chosen. A 0.16 in thumbscrew is permanently attached to the wing, which is inserted into the latch when the wing is attached. The latch is then locked in place, preventing lateral movement of the wing.

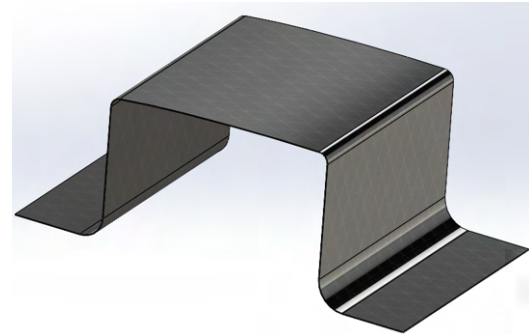


Figure 23: Wing Mount

### 5.3.5 Motor Mount

The motor mount was designed as a single 1/8 in thick carbon fiber plate joined to the carbon fiber sandwich panel fuselage skin using epoxy. The thickness of the plate was chosen to maximize the surface area for bonding the motor mount to the fuselage skin. The motor is bolted onto an X bracket which is then fastened to the motor mount plate, where washers are used to distribute the load. An FEA model was used to ensure the carbon fiber plate has sufficient strength to support thrust generated by the motor. Results indicate an expected deformation of 0.0003 in under max thrust with a maximum principle stress of 1,880 psi, well under the carbon fiber yield strength. Using the published shear strength of an epoxy joint between two carbon fiber surfaces, it was determined that the motor mount joint with the fuselage can safely withstand the maximum thrust of the motor.

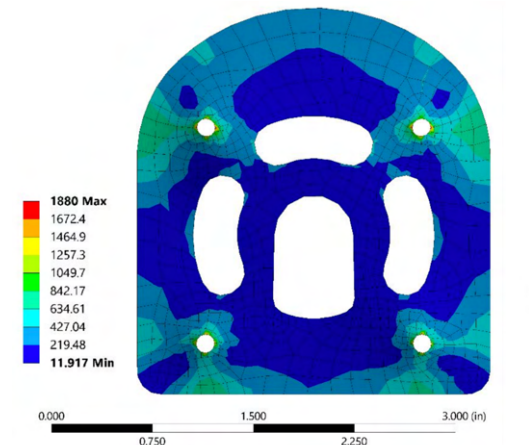


Figure 24: Motor Mount FEA Result

### 5.3.6 Empennage Connection

The fuselage and empennage are joined during assembly from the shipping container using a quick connect joint. During aerodynamic prototype testing, a structural failure occurred at the connection between the empennage and fuselage, resulting in a full hull loss of the flight vehicle. To eliminate future structural failures in this area of the fuselage, the loads at this point were reevaluated. The loads shown in Fig. 18 indicate shear force and bending moment at this point of 15 lb and 150 lb-in respectively. These loads were used for the design of the competition V1 and V2 fuselage-empennage interface. The quick connect joint consists of two 1/4 in plywood bulkheads bonded to the skin at the rear of the fuselage and the front of the empennage.

The connector has two spring-loaded retractable plungers embedded into 3D printed mounts on the bulkheads. These plungers latch onto radial grooves of pins embedded into the bulkheads. Four 0.24 in carbon rods run through both bulkheads to resist shear and torsion between the fuselage and empennage sections. Due to the critical nature of this component that became apparent after the aerodynamic prototype crash, each failure mode needed to be considered separately to ensure that loss of a competition aircraft would not come as a result of the interface's failure. The failure modes this joint can experience are outlined in Table 18 alongside the worst-case loads associated with M2 maneuvers and ultimate strengths each failure mode can withstand.

Table 18: Empennage Connection Failure Modes, Ultimate Strengths, and Operating Conditions

Potential Failure mode	Expected Operating Load	Design Loads & Stress
<b>Shear failure of epoxy bond between fuselage skin and bulkhead</b>	Max shear stress in epoxy bond of 30.4 psi	5 min cure Gorilla epoxy with 3300 psi shear strength when
<b>Shear Failure of carbon rods</b>	15 lb of shear force acting vertically in aircraft body frame	4 CF rods with x-section area will experience shear stress of 271 psi
<b>Failure of spring plunger and pin</b>	15 lb of shear force. 57.5 lb tension in each pin joint.	Pin lock system capable of withstanding 90 lb
<b>Failure of 3D printed mount</b>	57.5 lb of compression in each 3D printed mount	PLA has tensile strength of 5000 psi, 0.08 in <sup>2</sup> cross section will withstand 90 lb

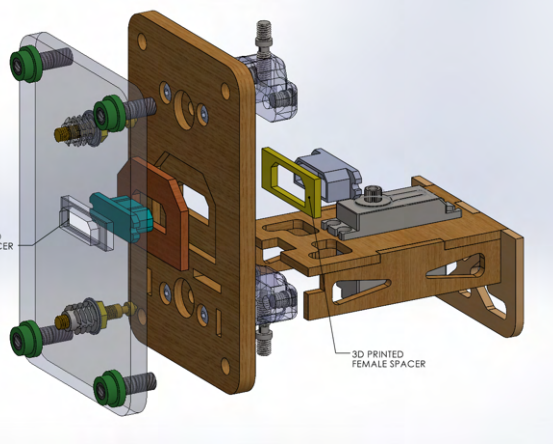
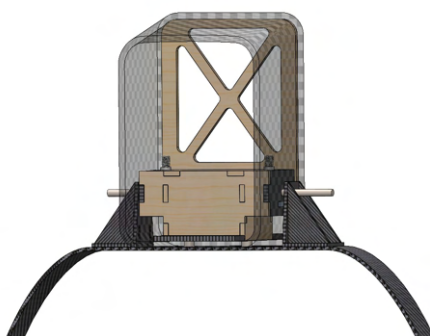


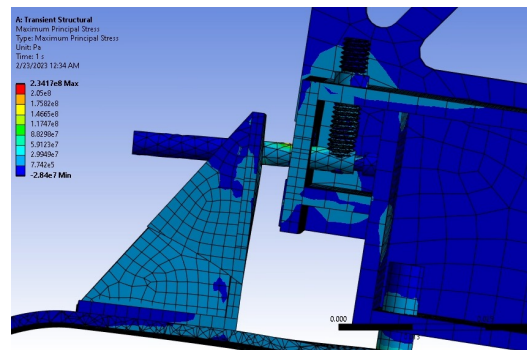
Figure 25: Empennage Connector

### 5.3.7 Landing Gear

An off-the-shelf carbon fiber strut was chosen to serve as the *Sailfin*'s main landing gear strut. Attached with two triangular carbon structures, the strut assembly was designed to be mounted onto the fuselage with 2 steel pins in the bottom and two steel locking pins through the sidewall and the triangular carbon structure, onto an internal mount. The steel pins and the carbon triangle allow fast assembly and low-profile storage space. The z-axis load is transferred from the interfacing top surface of the strut to the fuselage and all shear and bending moments are taken by the pins, transferring to the internal mount, as shown in Fig. 26a. The internal mount is constructed with carbon plates and plywood panels taking the compression load and dispersing the load from the landing gear to the fuselage. An FEA was conducted on the main landing gear assembly with 10g loading in the x and z axis respectively based on a recorded maximum landing acceleration of 7g. The result, as shown in Fig. 26b, shows stress concentration on steel pins, but the FoS was still 2 given the loading case. A set of F3A-compatible wheels and axles were chosen to comply with storage space requirements.



(a) Landing Gear Assembly



(b) Landing Gear FEA

Figure 26: Main Landing Gear

The rear landing gear was designed for fast assembly. An off-the-shelf tail wheel assembly is mounted onto a 3D printed nylon mount that aligns with the shape of the horizontal stabilizer. As shown in Fig. 27, the mount has two holes for the horizontal stabilizer spars to pass through, fixing the mount to the fuselage. The rear landing gear has control rods attached to the rudder for steering.



Figure 27: Rear Landing Gear Mount

### 5.3.8 Tail

The horizontal stabilizer is made with an XPS foam core covered in one layer of 45 degree spread tow carbon fiber to provide rigidity. The horizontal stabilizer contains two carbon fiber spars to carry the aerodynamic loads to the skin of the fuselage. The main spar is a 0.39 in carbon fiber spar located at 25% of the chord length from the leading edge, and it spans the entire length of the horizontal stabilizer. The secondary spar has a diameter of 0.24 in and is located at 45% of the chord length from the leading edge, spanning 25% of the horizontal stabilizer length. The purpose of the main spar is to carry the lift and drag forces, while the secondary spar exists to counteract aerodynamic moments. The spar diameters were chosen after analyzing the expected loads the horizontal stabilizer will undergo during flight. Specifically a predicted distributed load equal to 19.78 lb of lift and 1.35 lb of drag. Since the large control surfaces on the *Sailfin* required powerful servos, Kevlar hinges were chosen for both the elevator and rudder in order to account for the larger servo forces. The horizontal stabilizer's connection to the empennage was designed to minimize assembly time during competition. MPX6 connectors are used for wiring to provide a quick connection. The vertical stabilizer consists of two parts, a static section built into the fuselage, and a rudder, making up 45% of the chord. The static section

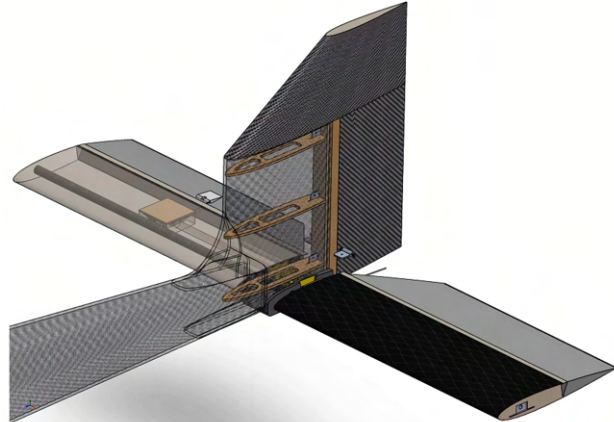


Figure 28: Tail Detail Design

of the vertical stabilizer also contains 3 wood ribs for additional support. The horizontal stabilizer is an XPS foam core wrapped in one layer of 2.36 oz/yd<sup>2</sup> spread tow carbon fiber. The rudder is actuated using pull-pull rods and a KST X15-1809 servo located at the front of the empennage. The servo's location at the connection of the empennage to the fuselage was dictated by weight and balance considerations.

### 5.3.9 Antenna Mount

The antenna adapter is a friction-fit “cup holder” that can be bolted into the aircraft’s wingtip. The piece was made from 3D printed PETG and uses two 1/4"-20 machine screws to fasten to the wing’s box beam. The piece was designed to be light-weight, aerodynamic, and as thin as possible in order to maximize the M3 score and reduce impact on the aircraft’s flight characteristics. After testing different adapter heights, 0.6 in was settled on as the proper balance between reducing height while maintaining reliability. The fasteners are 1.5 in apart center-to-center.

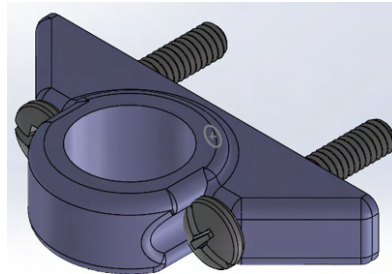


Figure 29: Antenna Mount

### 5.3.10 Ground Mission Test Fixture

The GM test stand design was inspired by sawhorses to create a simple, stable and easy to manufacture structure. Each stand consists of an A-frame on top of a plywood base. These two stands are then held together by a 2x4 board. The plywood base is loaded with weights to counteract the moment caused by loading the aircraft, creating a more stable base. For the wing interface, a hinge mount was chosen to create a pinned-pinned beam system. This was determined to be better than a fixed-fixed system because it removed moment stresses from the wing tip. The fasteners are 1.5 in apart center-to-center to secure to threaded inserts in the wing’s box beam. Although narrow, it was decided attaching to a solid point was more important than spreading out the bolts to improve stability. The bolts used were 1/4in-20 Phillips-slotted combination machine screws. The full structure is shown in Fig. 30.

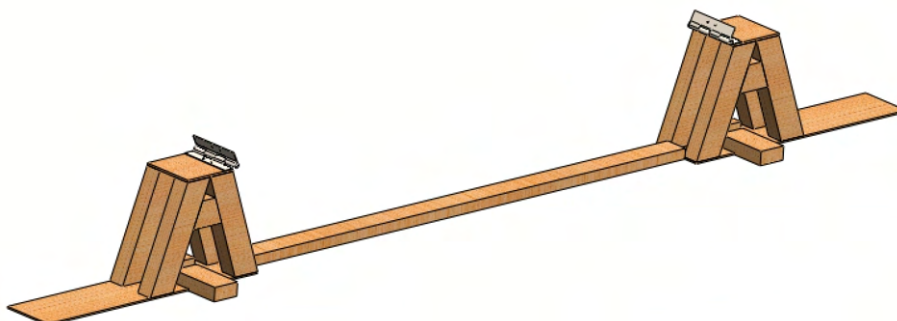


Figure 30: Ground Mission Test Fixture

### 5.3.11 Shipping Container

The transport box is made with 2510 prepreg carbon fiber, aluminum hinges, ABS plastic, and magnets. Because the priorities for the box were to ensure maximum usable volume with the given dimensions of 38 in length, 13 in height, and 11 in width, prepreg was determined to be the optimal material for the box walls due to its small thickness and high rigidity. The walls consist of two layers of prepreg oriented at 45 and 90 degrees. The angle brackets holding the separate panels together consist of three layers of prepreg, with the outside layers oriented in opposing directions. A custom-designed shipping box was deemed necessary over a commercially available container because a custom box allows for a more efficient use of volume and provides more flexibility for the wingspan, antenna, and fuselage lengths. Additionally, the custom box was designed with accessibility in mind, the main feature being the ability to unroll. This feature was implemented to provide quick access from the top and side during assembly, which will assist in meeting the mission time limits. Fig. 31 shows the shipping container loaded with all aircraft parts.

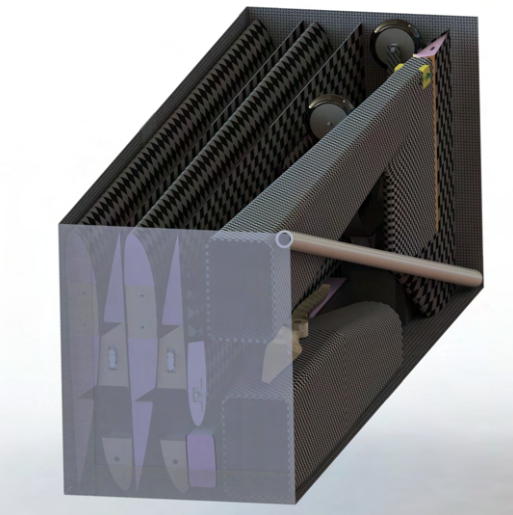


Figure 31: Shipping Container Loaded

### 5.3.12 Propulsion

From further performance analysis and propulsion tests, the APC 16X12E propeller was selected as the primary propeller for the final aircraft due to its sufficient thrust, enabling target flight speeds for all flight missions. On the other hand, the motor, ESC, and battery of the propulsion system were unchanged from the preliminary design shown in Table 13.

### 5.3.13 Avionics

To assist the pilot and the aircraft's performance, various stabilization and sensor systems were considered. Based on the team's needs and support from technology sponsors, the avionics system was configured as shown in Table 19.

Table 19: Avionics Component Table

Flight Controller	Avionics Battery	Servo	Servo PDB
MATEK H743-SLIM-V3	1300mAh/1100mAh 3s 35C LiPo	KST X10mini	MATEK SERVO PDB W/ BEC
Current Sensor	Voltage & RPM Sensor	Airspeed Sensor	Receiver
MATEK Hall Current Sensor 150A	APD 120A F3[X]	MATEK ASPD-4525	FrSky R-XSR

The Matek H743-SLIM flight controller was selected for its telemetry, black box, and stabilization functionalities in a small and light form factor. A Matek ASPD-4525 airspeed sensor, a Matek Hall 150A current sensor, and two FrSky R-XSR receivers are connected to the flight controller, completing the avionics suite. For maximum safety, the Frsky receivers are connected in redundancy mode so that if one receiver triggers fail-safe, the other receiver will assume control until both receivers fail-safe. Lastly, the avionics battery was chosen such that all avionics have sufficient power to function for the duration of each mission while minimizing the weight. Based

on the maximum energy consumption of all components, a 3S 1300 mAh LiPo was selected for M2, and a 3S 1100 mAh LiPo was selected for M1 and M3, both with a minimum discharge rate of 35C.

### 5.3.14 Wiring

To reduce wiring weight and increase repair ability, the flight controller only transmits servo signal, with no servo power passing through it. Servos are powered by dedicated PDBs directly connected to the avionics battery, and they run at 7.2 V to provide sufficient torque. A series of ribbon wires mounted on the side wall deliver signal from the flight controller to the PDBs, while two flat copper wires located on the opposite side wall deliver power. To connect servos on each wing section and horizontal stabilizer to the fuselage, a pair of MPX6 connectors are hard mounted on the root of the wing and fuselage. A pair of JX9 connectors are hard mounted at the joint interface of the fuselage and empennage section, connecting 3 servos and a pair of receivers. The choice to hard mount was made to improve assembly time since the connectors lock with the structures.

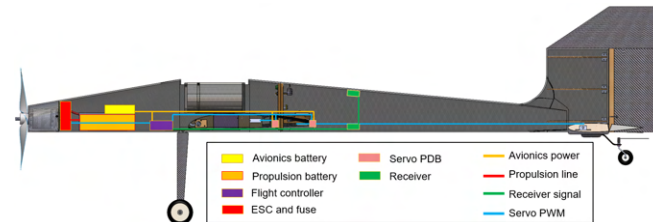


Figure 32: Wire Routing Diagram

### 5.3.15 Control Surface Linkage and Drive System

To increase packing efficiency, integrate drive system (IDS) linkages are employed on the *Sailfin*. The IDS comprises of an internal linkage with a special attachment to the control surface opposite to the hinged side. This eliminates the protrusion on the surfaces of the wing by the servo arms and control horns, significantly reducing the space taken by the four wing sections in the box.



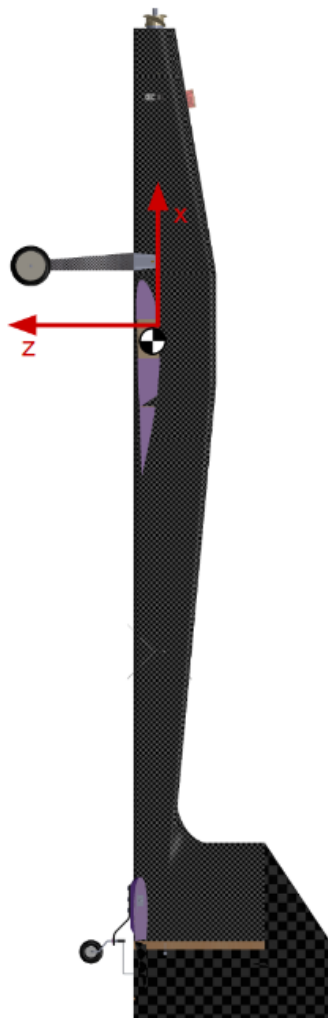
Figure 33: An IDS Assembly

## 5.4 Weight and Balance

The weight and balance of the *Sailfin* was analyzed by using measured weights of off-the-shelf components, measured weights-per-unit-area of composite materials such as honeycomb carbon fiber sandwich panels, and estimated weights based on volume and density. All three of these techniques are used in conjunction with SolidWorks 22 CAD software to determine the location of each component in a reference frame centered at the 1/4 chord of the wing and along the aircraft's thrust axis. Table 20 summarizes the weight and balance analysis by showing the weight of all main subsystems and large components and their locations with respect to the given reference frame. All three payload configurations are considered.

Table 20: Weight and Balance Table with Vehicle Reference Frame

Component	Weight (lb)	X Displacement (in)	Z Displacement (in)
Propulsion Battery	1.61	+13.58	+0.27
Avionics Battery	0.22	+11.58	+0.45
Motor	1.23	+15.52	+0.45
Propeller	0.08	+19.87	0.00
Flight Control Electronics	0.52	-9.61	+0.50
Wiring	0.27	-10.26	+0.09
Wing Structure	2.67	-1.66	+0.36
Nose Tapered Section	0.32	+8.60	-0.69
Fuselage Midsection	0.28	-2.00	-1.31
Empennage Section	0.73	-24.50	-0.37
Empennage Connection	0.47	-6.61	-0.61
Motor Mount	0.10	+15.99	-0.30
Wing Mount	0.37	+0.30	+0.37
Main Landing Gear	0.74	+4.16	+4.98
Tail Landing Gear	0.25	-38.03	-2.00
Horizontal Stabilizer	0.41	-36.96	+0.86
Vertical stabilizer	0.15	-37.65	-3.57
Glue	0.20	0.00	0.00
<hr/>			
Electronics Package	9.33	0.00	-2.31
Antenna	0.52	0.00	+19.00
Antenna Counter-Weight	0.52	0.00	+0.17
Antenna Mount	0.20	0.00	+0.17
	Weight (lb)	X CG (in)	Z CG (in)
M1	10.61	-1.08	+0.41
M2	19.94	-0.57	-0.86
M3	11.85	-0.96	+1.21



## 5.5 Predicted Aircraft Flight and Mission Performance

## 5.6 Drawing Package

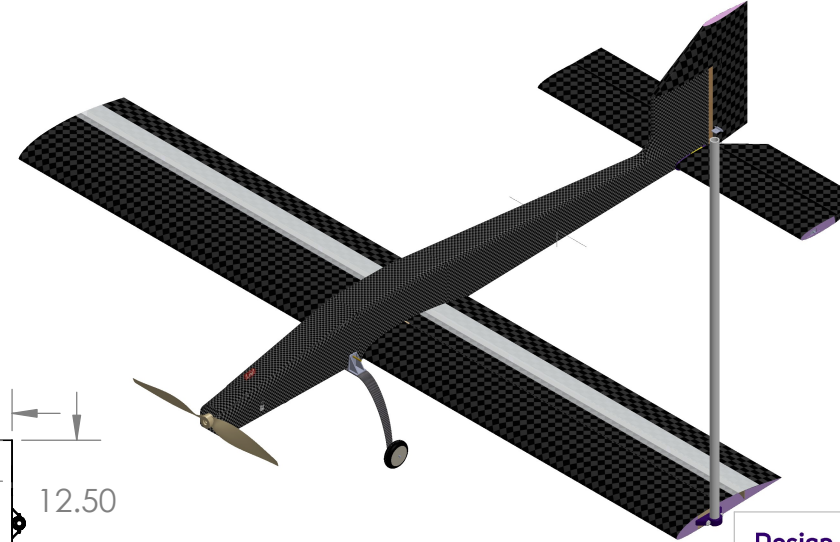
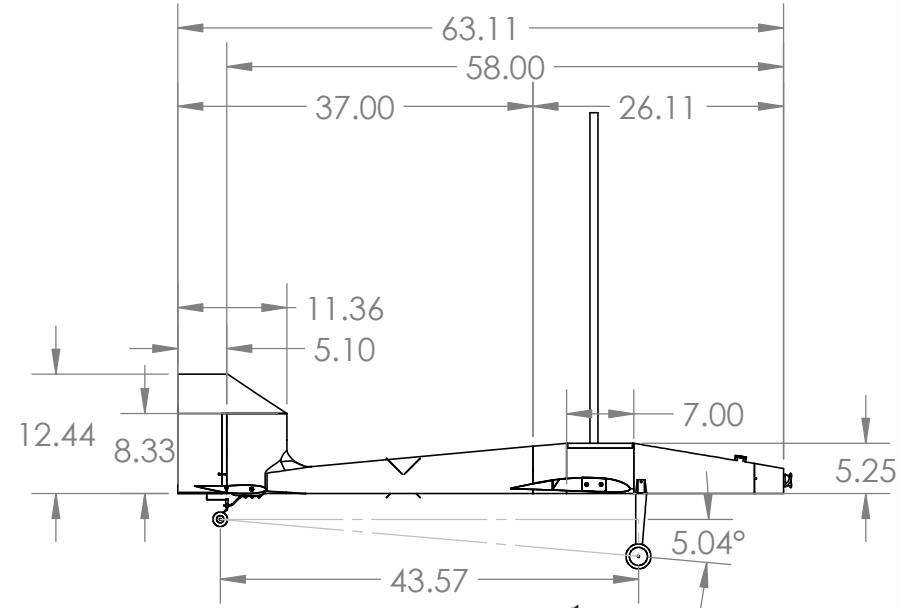
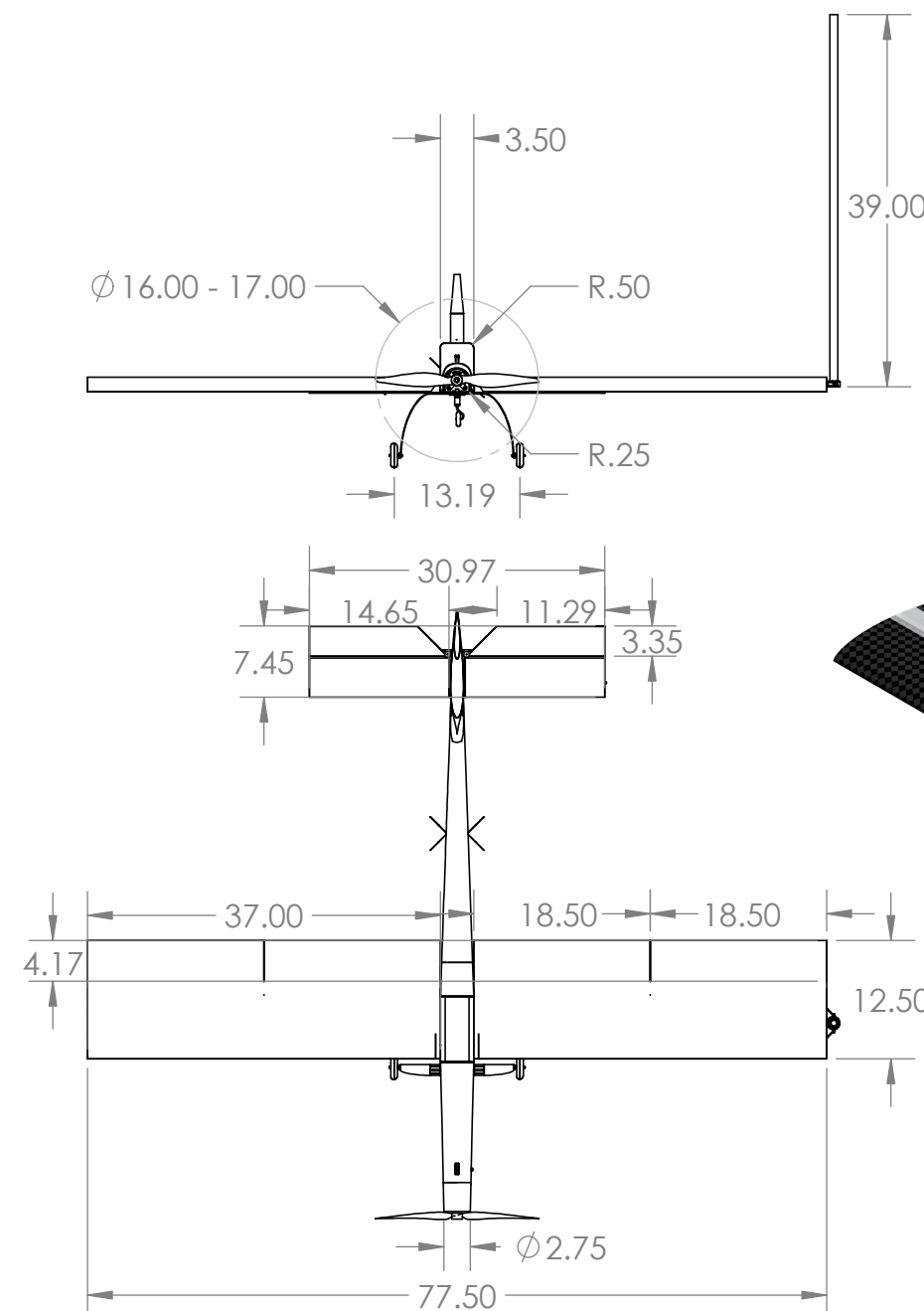
The drawing package contains a dimensioned 3-view of the aircraft, exploded views of the primary structure of the aircraft, locations of the electronics within the aircraft, and detailed views of the subsystems of the aircraft.

2

1

B

B



<h1>Design Build Fly</h1> <p>at the University of Washington</p>		
<small>UNLESS OTHERWISE NOTED: DIMENSIONS ARE IN INCHES</small>	 <h2>HuskyWorks</h2>	
<h2>University of Washington AIAA Design Build Fly 2023</h2>		
<b>TITLE:</b>	Sailfin	
<b>SIZE</b>	DWG. NO.	REV
<b>A</b>	Aircraft 3-View	<b>A</b>
<b>SCALE:</b> 1:20		Drawing Package
SHEET 1 OF 4		

2

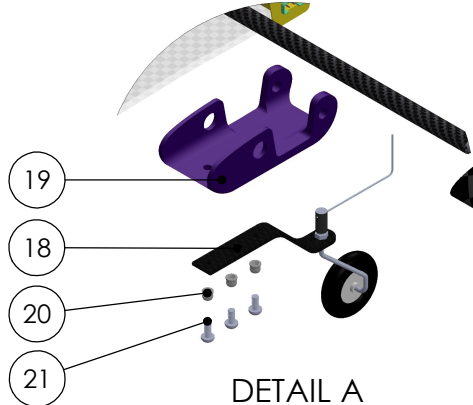
1

2

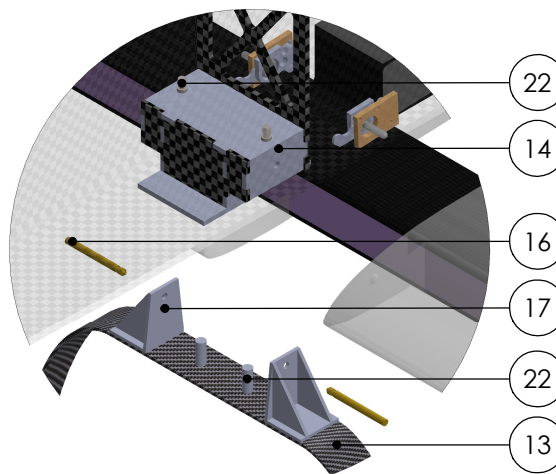
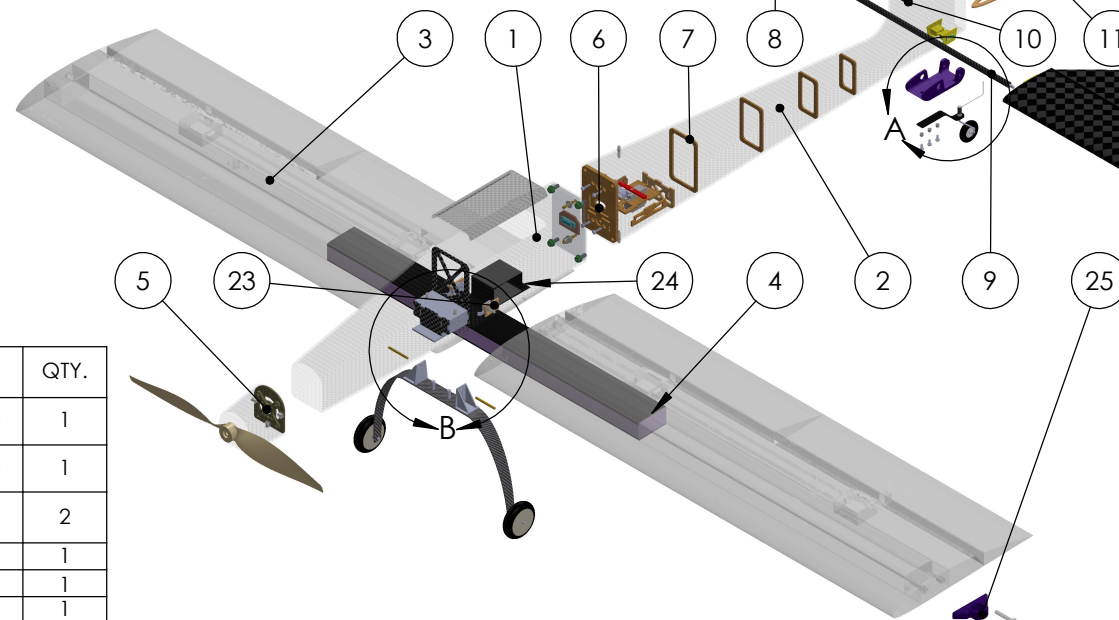
1

B

B



Item NO.	Name	Description	QTY.
1	Fuselage	CFRP / Aramid Honeycomb	1
2	Empennage	CFRP / Aramid Honeycomb	1
3	Wing + Control Surfaces	CFRP / XPS-foam / Balsa / Plywood / Kevlar	2
4	Wing Spar	CFRP / XPS-foam	1
5	Motor Mount	CFRP	1
6	Emp-Fuse Connector	CFRP / Nylon	1
7	Empennage Ribs	Plywood	4
8	Elevators + H-Stab	CFRP / XPS-foam / Kevlar	1
9	H-Stab Main Spar	CFRP	1
10	H-Stab Secondary Spar	CFRP	1
11	V-Stab	CFRP / Aramid Honeycomb / Balsa	1
12	Rudder	CFRP / XPS-foam	1
13	Main Landing Gear	CFRP	1
14	Main Landing Gear Mount	CFRP / Plywood	1
15	Vertical Pins	Steel	2
16	Horizontal Pins	Steel	2
17	Landing Gear Truss	CFRP	2
18	Tail Landing Gear	CFRP	1
19	Tail Mount	Nylon	1
20	Heated Insert	Steel	3
21	M4 Screw	Steel	3
22	Spring Plungers	Steel	2
23	Wing Latch Lock	Aluminum	2
24	Wing Spar Mount	CFRP	1
25	M3 Mount	PETG	1

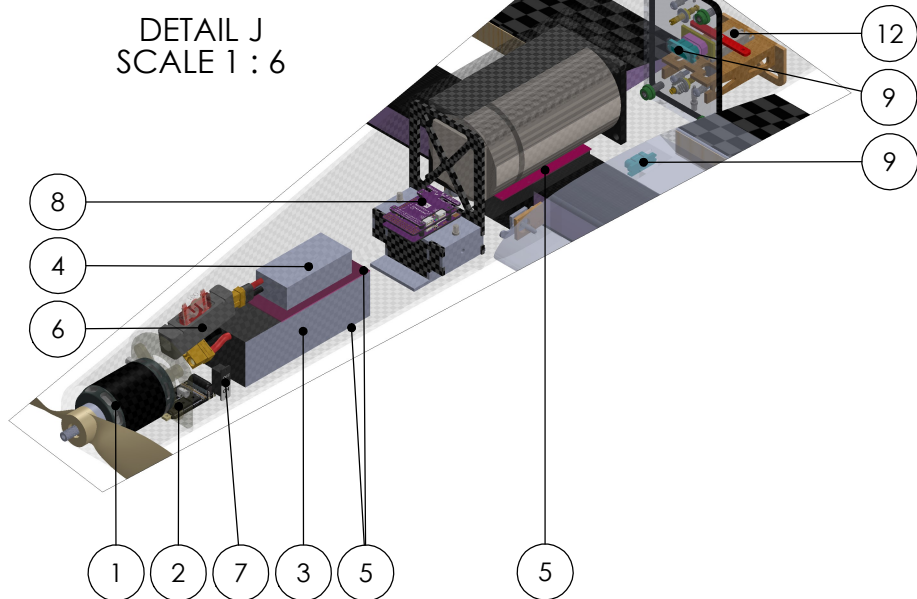
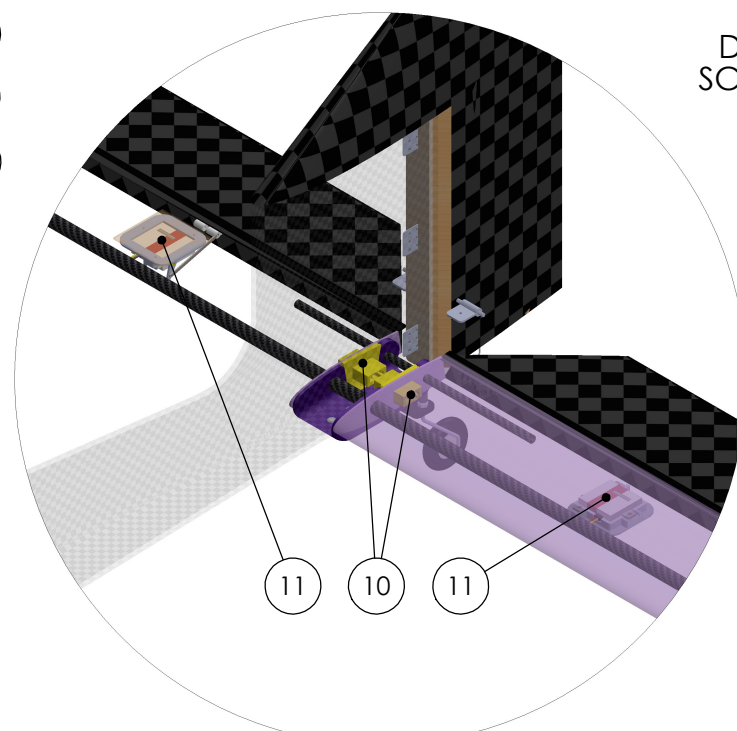


2

1

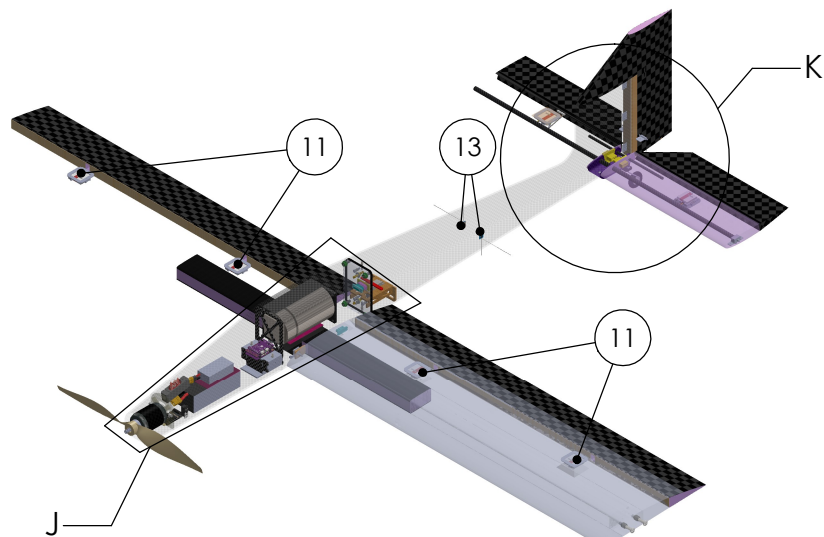
2

1

DETAIL J  
SCALE 1 : 6DETAIL K  
SCALE 1 : 5

B

B



A

A

Item NO.	Name	Description	QTY.
1	Motor	T-Motor 4140	1
2	ESC	APD 120F3x	1
3	Propulsion Battery	8s LiPo	1
4	Avionics Battery	3s LiPo	1
5	Sticky Pad	Umma Grip Lite	3
6	Fuse	MAXi Blade 100A	1
7	Avionics Switch	Spektrum Deluxe 3	1
8	Flight Controller	Matek H743-SLIM	1
9	9 Pin Plug Set	JX9	3
10	6 Pin Plug Set	MPX6	2
11	Wing / Elevator Servo	KST X10 mini	6
12	Rudder Servo	KST X15-1809	1
13	Receiver	FrSky R-XSR	2

**Design Build Fly**  
at the University of Washington  


UNLESS OTHERWISE NOTED:  
DIMENSIONS ARE IN INCHES HuskyWorks

University of Washington  
AIAA Design Build Fly 2023

TITLE: Sailfin

SIZE DWG. NO. REV

A Systems View A

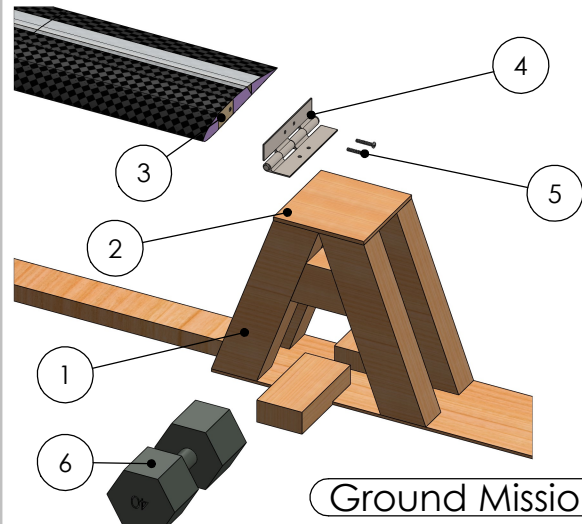
SCALE: 1:16 Drawing Package SHEET 3 OF 4

2

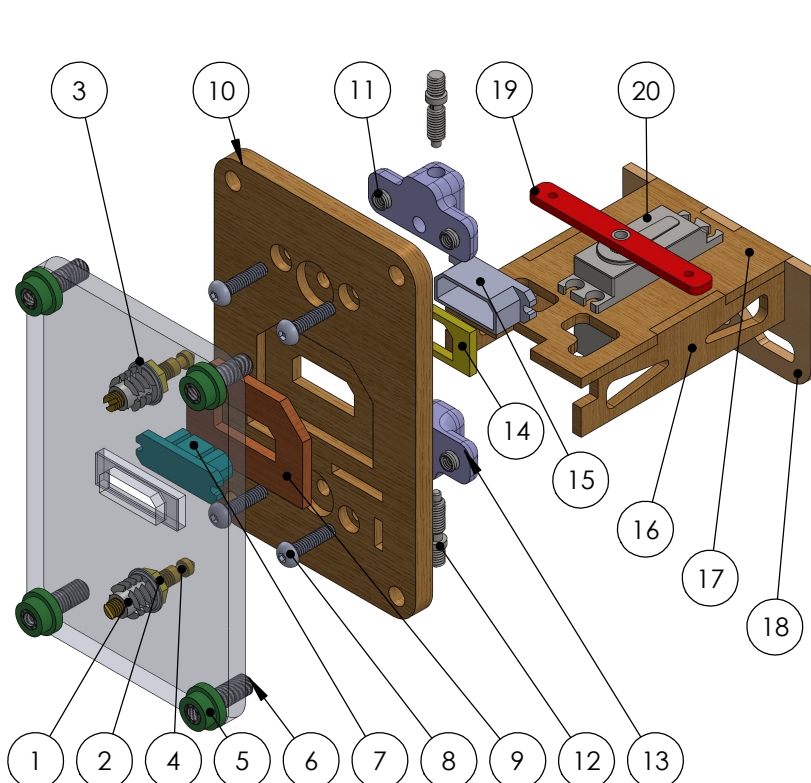
1

B

B



ITEM NO.	Name	Description	QTY.
1	Support Structure	Wood	NA
2	Support Panels	Plywood	NA
3	Insert	Steel	4
4	Hinge	Steel	2
5	Bolt	Steel	4
6	Weights	Steel / Sand	NA



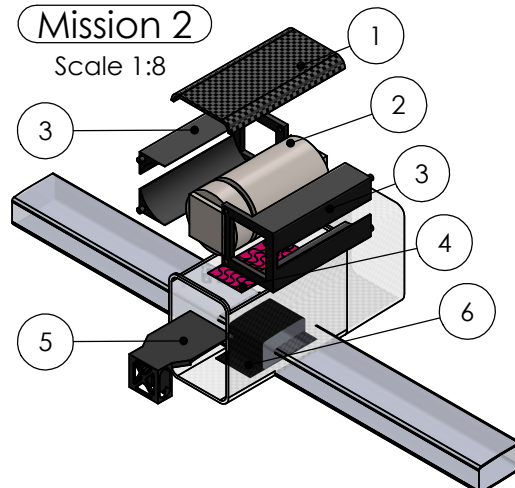
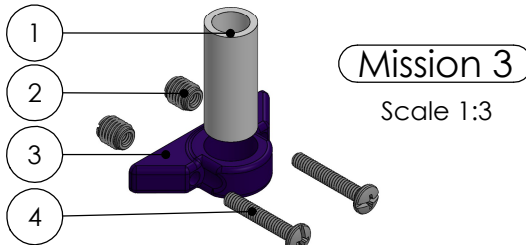
Scale 1:2

ITEM NO.	Name	Description	QTY.
1	Insert	Steel	2
2	Nut	Steel	2
3	Washer	Steel	2
4	Locking Pins	Steel	2
5	Dowel Aligner	PLA	4
6	Dowels	CFRP	4
7	9 Pin Plug (M)	Plastic	1
8	M4 Screw	Steel	4
9	Plug Aligner	Plywood	1
10	Interface Plate	Plywood	2
11	Heated Insert	Brass	4
12	Spring Plunger	Steel	2
13	Plunger Holder	Nylon	2
14	Plug Spacer	PLA	1
15	9 Pin Plug (F)	Plastic	1
16	Servo Mount	Plywood	2
17	Servo Mount	Plywood	1
18	Servo Mount	Plywood	1
19	Servo Arm	Aluminum	1
20	Rudder Servo	KST X15-1809	1

A

A

Item NO.	Name	Description	QTY.
1	PVC Pipe	39 inches	1
2	Tapping Insert	Steel	2
3	M3 Mount	PETG	1
4	Bolt	Steel	2



ITEM NO.	Name	Description	QTY.
1	Payload Hatch	CFRP	1
2	Payload	Steel	1
3	Payload Shell	Nylon	2
4	Sticky Pad	Umma Grip Lite	1
5	Payload Mount	Nylon	1
6	Wing Spar Mount	CFRP	1

Drawn By:  
Enoch KwongDate Drawn:  
2-23-23Design Build Fly  
at the University of WashingtonUNLESS OTHERWISE NOTED:  
DIMENSIONS ARE IN INCHES

HuskyWorks

University of Washington  
AIAA Design Build Fly 2023

TITLE: Sailfin

SIZE DWG. NO. REV  
**A** Mission Critical **A**

SCALE: 1:15 Drawing Package SHEET 4 OF 4

2

1

## 6 Manufacturing Plan

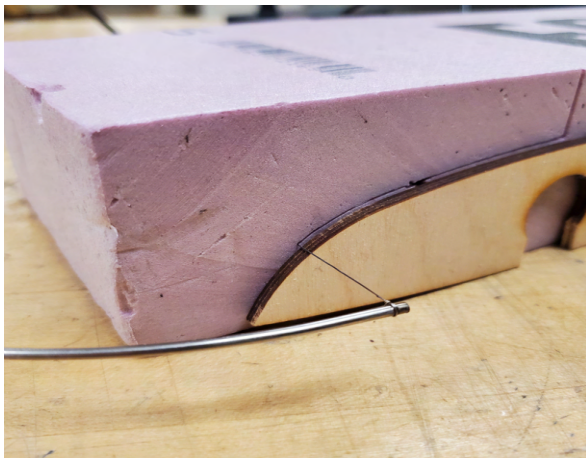
The following section describes the manufacturing of the *Sailfin*, breaking down the manufacturing processes used to build the aircraft, and the timeline for getting all components and spare parts built and assembled.

### 6.1 Manufacturing Processes Descriptions

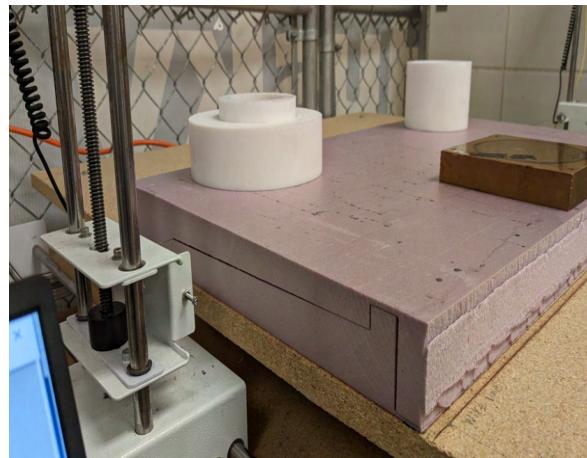
The processes in Fig. 21 are described in this section as well as additional processes used in the post-processing of parts, or general manufacturing of the aircraft such as CAD model exports.

#### 6.1.1 Hot Wire Cutting Foam

Based on the team's experience and confirmed by a recommendation from subject matter experts, it was determined that hot wire cutting of XPS foam was superior to any other method available for 2-D applications. Further discussion determined that CNC hot wire cutting would require extra diligence and time to set up. On that basis, its use was reserved for final products. Prototypes of 2D foam shapes were generally cut by hand using laser cut plywood cutting templates as necessary. As designs matured and the team's skill using the CNC hot wire cutter evolved, the final few prototypes were cut using the CNC cutter. A program called DevFoam was used to manipulate 2D profiles defined by a DXF in a simulated foam cutting environment before converting to gcode and cutting.



(a) Hot Wire Cutting by Hand Using a Plywood Stencil



(b) CNC Hot Wire Cutter in Action

Figure 34: Hot Wire Cutting Methods

#### 6.1.2 Laser Cut Parts

Based on previous experience, laser cutting was determined to be the fastest way to manufacture 2D plywood parts. Simple parts can be cut in under 5 minutes. The laser can have the illusion of creating incredibly precise parts, while if not calibrated correctly can actually be causing significant errors. To mitigate this issue, parts were measured using calipers after cutting and compared to CAD dimensions to ensure they remained to spec. If errors were discovered, the laser was recalibrated and tested to ensure it was back to cutting accurate parts.

### 6.1.3 3D printing

3D printing was determined to be the most efficient method for creating complex 3D geometry where structure is not a concern. Parts such as cowlings, adapters, or ergonomic interfaces fall into this category. 3D printing allows for easy weight management because the infill of parts can be changed easily in a slicer. Additionally, 3D printing requires minimal hands-on work while manufacturing. A print can be started and run for several hours without the need for engineer interaction. This allows engineers to focus their efforts on other components of the aircraft and can speed up manufacturing. For 3D printed parts, Prusa Slicer was used to convert STL files into gcode files for the team's Prusa MK3s 3D printer.

### 6.1.4 Composite Layups

Composite research and experimentation has been a focus of the team for the past 4 years. With several years of experience, the team felt confident to manufacture composite parts that outclass the strength-to-weight ratio of other methods, such as balsa wood and covering film manufacturing. While the complexity and time required to build composite parts was of concern, subject matter experts recommended that the structural requirements of the GM warranted the use of composite structures to maximize score. The risk to manufacturing timelines and quality was accounted for by implementing quality assurance checks and dedicated training and experimentation time before the manufacturing cycle. Both vacuum bagging and un-bagged layups were used. Vacuum bagged layups were used for most parts, requiring vacuum pressure to force the composites to the core shape. Complex parts were made with prepreg carbon fiber cured in an autoclave was used to optimize composite weight and strength.

### 6.1.5 CNC Machining

CNC machining was used for 2D parts that could not be cut on a laser and required high accuracy (See Fig. 21). CNC machining was determined to be superior to either cutting parts by hand or water jet cutting. Cutting parts by hand was not feasible for the experience level of our members and the complex shapes to be cut, such as the motor mount. Water jet cutting was not viable because parts were not within the material thickness limitations. CAM for CNC machined parts was created in Fusion 360 because of member experience with the software.



Figure 35: CNC Router Cutting Fuselage Mold

## 6.2 Manufacturing Overview

### 6.2.1 Fuselage

The fuselage was built using a vacuum bagged, negative molded composite layup. The fuselage was made in two halves, splitting the fuselage vertically from nose to tail. Each half was laid up in a separate mold with 2 layers of spread tow carbon fiber sandwiching one layer of 1/8 in aramid honeycomb core, and an additional 2 layers of carbon fiber in some areas for reinforcement. The layup was held under vacuum pressure for approximately 6 hours and cured for a total of 24 hours before post processing began. The two halves were trimmed with a Dremel tool to create a flush seam, and plywood ribs were epoxied into one side using a jig as shown in Fig. 36. The halves were then sealed together using strips of carbon fiber lapping over the external joints and additional epoxy on the exposed side of the ribs. Finally, hatches were cut using a Dremel tool and excess carbon was removed via sanding. After the evaluation of the V1 aircraft, the team decided to switch to prepreg carbon fiber for increased rigidity and strength. Which involves the use of an autoclave.



Figure 36: Jig for the Fuselage Ribs



(a) Wet Layup



(b) Vacuum Bag

Figure 37: Composite Manufacturing

### 6.2.2 Wings

The wings were built by starting with CNC hot wire cutting the XPS foam cores for the spars. The cores were then laid up with 5 layers of unidirectional carbon fiber on the top and bottom. This layup was vacuum bagged and held under vacuum pressure for approximately 3 hours before curing for 24 hours. For the wings, a dummy block of foam wrapped in release film was added to the foam core and laid up on top of to create a slot for the center wing spar to insert.

The leading edge was cut from XPS foam with the CNC hot wire cutter and bonded to the front of the outboard spar using foam glue. The trailing edge was similarly bonded to the outboard spar and also made using XPS foam. To ensure proper alignment a mold was cut from XPS foam allowing for all of the individual segments of the wing to be assembled and glued into their final shape. This entire assembly was wrapped in a layer of carbon fiber spread tow to complete the aerodynamic surface. Cavities for servos and wires were cut using a router attachment on a Dremel tool. This process was repeated for all 4 wings.



Figure 38: Wings Curing in the Vacuum Bag

### 6.2.3 Tail

The vertical stabilizer was integrated into the layup of the fuselage, and laser cut plywood ribs were epoxied to the internal carbon fiber shell. Plastic hinges were used to attach the rudder to these ribs, which was made of a manual hot wire cut XPS foam core wrapped in a fiberglass layup. The core was cut manually because the complex two part shape of the rudder could not be cut on the CNC hot wire cutter. The horizontal stabilizer was built with a CNC hotwire cut XPS foam core wrapped in a single layer of spread tow carbon fiber. Plywood end plates were laser cut and glued to the ends of the stabilizer and the elevator was attached with a separate layup of the Kevlar hinge. Cavities for servos and wires were cut using a router attachment on a Dremel tool.

### 6.2.4 Payloads and Mission Mounts

The competition electronics package was made of a stainless steel core and 3D printed PETG plastic exterior. The steel core was cut to size using a hacksaw, and glued into the 3D printed package. The mount for the electronics package was also 3D printed in PETG plastic, and print layers were intentionally orientated parallel to the floor of the fuselage to maximize compressive strength. The antenna mount adapter was 3D printed from PETG plastic. The antenna itself was cut to length using a hacksaw. The GM test stands were built in the team's wood shop, using a compound miter saw to cut lumber to length and create miter joints for easy assembly. Plywood was cut to size using a table saw, and the entire assembly was completed using wood screws and an impact driver. The transport box was made with 2510 prepreg carbon fiber, aluminum hinges, ABS plastic, and magnets. Instead of an autoclave, the prepreg carbon fiber flat panels were cured on a heat press. The walls were made of two layers of prepreg oriented in a 45-90 layup; the 38 in length walls were split diagonally into two trapezoids due to the size constraints of the composite heat press. The angle brackets holding the separate panels together consisted of three layers of prepreg, with the exterior layers oriented in opposing directions. This process began by using a CNC fabric cutter to cut panels at 45° and 90° to the weave, which were then laid on top of each other. The angle brackets were manufactured using a vacuum-mold process. This process consisted of hand-cutting prepreg and laying it over a foam mold. These parts were then vacuum-sealed and placed in an autoclave where they were cured. The panels and angle brackets were then epoxied together to

form the transport box. Four panels were fixed in place via the angle brackets, while two of the panels were attached via hinges. Latches and magnets were also attached with epoxy to hold the hinged panels in place.

### 6.2.5 Summary

The manufacturing strategy for each component of the aircraft is summarized in Table 21. Fig. 39 shows the materials used in the construction of the *Sailfin*.

Manufacturing			
Aircraft component	Parts	Materials	Processes
Fuselage	Skin	Nomex honeycomb (1/8") Carbon fiber prepreg	Autoclave Cure
	Ribs	Plywood (1/8" birch)	Laser cut
Propeller Assembly	Purchased including propeller, spinner, and attachement hardware (APC)		
Motor	Purchased including attachement hardare and mounting plate (TMOTOR)		
Battery	Purchased (SMC)		
Fuse	Purchased (Amazon)		
Landing Gear	Carbon Gear		Purchased (Hobbyking)
	Mount	Plywood (1/8" birch)	Laser cut
		Carbon fiber panel (1/8")	CNC machined
		PETG filament	3D printed
Vertical Tail	Skin	Nomex honeycomb (1/8") Carbon fiber (45°, 2.36 oz spread tow)	Vacuum bag layup
	Ribs	Plywood (1/8" birch)	Laser cut
	Rudder	Foam (XPS Foamular NGX F-250)	Hotwire cut (by hand using laser cut templates)
		Fiberglass (0.75 oz plain weave)	Hand layup
Horizontal Tail	Skin	Carbon fiber (45°, 2.36 oz spread tow)	Hand layup
	Core	Foam (XPS Foamular NGX F-250)	Hotwire cut (CNC)
	End plates	Plywood (1/8" birch)	Laser cut
Wings	Spar	Foam (XPS Foamular NGX F-250)	Hotwire cut (CNC)
		Carbon fiber (unidirectional)	Hand layup
		Carbon fiber (45°, 2.36 oz spread tow)	Vacuum bag layup
	Skin	Carbon fiber (45°, 2.36 oz spread tow)	Vacuum bag layup
	Core	Foam (XPS Foamular NGX F-250)	Hotwire cut (CNC)
Avionics	Flight controller		Purchased (MATEKSYS)
	Wiring	Servo wires	
		Propulsion wires (12 awg)	Soldering
	ESC		Purchased (APD)
Electronics Package	Weight	Steel	CNC Milled
	Box	PETG Filament	3D printed
	Mount	PETG Filament	3D printed
Jamming Antenna	Mount	PETG Filament	3D printed
	Antenna	1/2" Schedule 40 PVC pipe	Purchased (Home Depot)
Ground Mission	Test stand	Lumber (Fir)	
		Plywood (3/4")	Wood working
	Adapter	Metal hinges	Purchased (Home Depot)

Table 21: Manufacturing Details Including Materials and Processes Used Broken Down by Aircraft Component

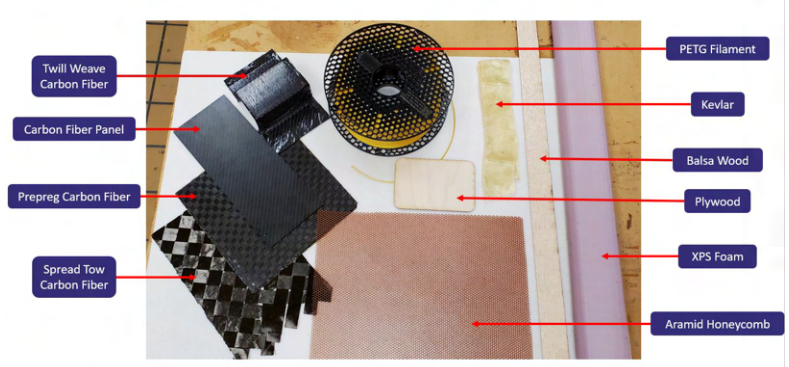
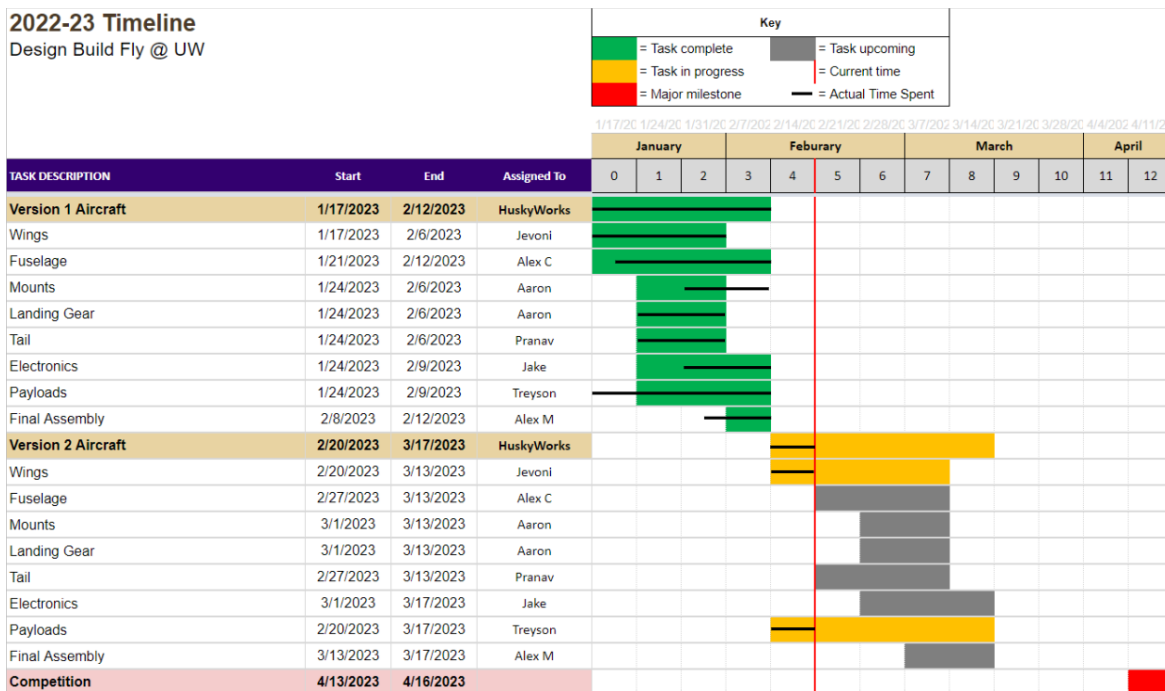


Figure 39: Materials Used in Manufacturing

### 6.3 Manufacturing Schedule

The manufacturing schedule for the *Sailfin* is shown in Fig. 40. Several iterations of the aircraft were built, and all followed the same outline as the one shown for the final aircraft in Fig. 40.

Figure 40: Manufacturing Schedule for the Final Iteration of the *Sailfin*

## 7 Test Plan

A variety of tests were conducted on the aircraft's materials and components throughout the year. The goal was to validate predicted performance and inform design decisions through analysis of acquired data.

## 7.1 Test Schedule

To manage all testing throughout the year, the timeline shown in Fig. 41 was developed to keep track of progress.

**2022-23 Testing Timeline**

Design Build Fly @ UW

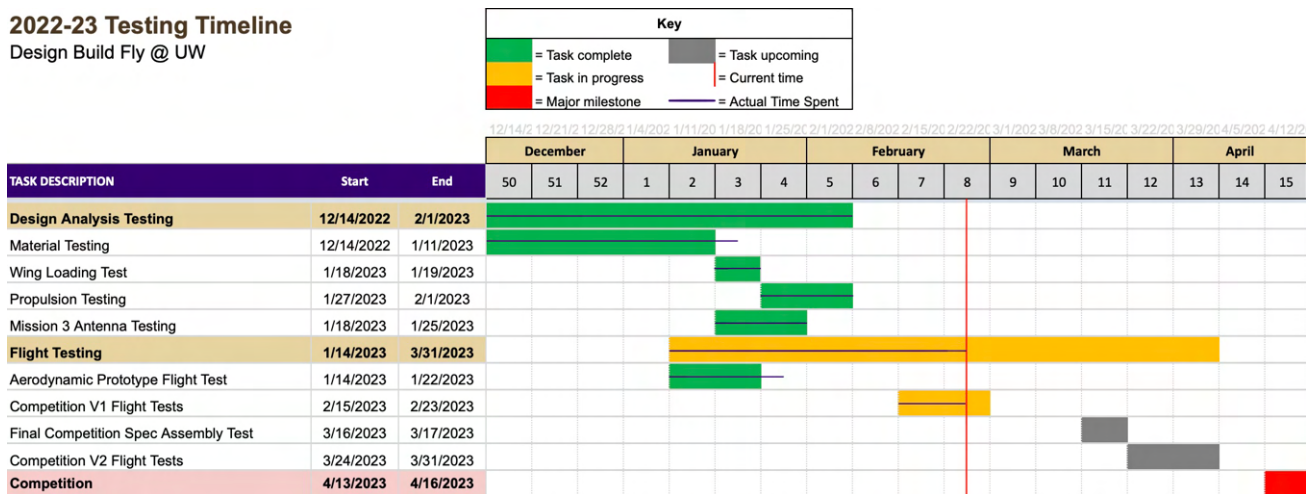


Figure 41: Testing Timeline Gantt Chart

## 7.2 Testing Objectives

The tests performed were split into two categories: design analysis testing, and flight testing. Design analysis testing included aerodynamic testing, structural testing, and static propulsion testing. The goals were to validate aircraft performance prior to getting into the air. Flight testing included testing of three air frames: an aerodynamic prototype, a competition Version 1 (V1) aircraft, and a competition Version 2 (V2) aircraft. All testing was used for design iterations and improvements, and verification that requirements were met.

## 7.3 Design Analysis Testing

### 7.3.1 Aerodynamic Testing

Due to technical difficulties, the University of Washington's wind tunnel was unable to support the HuskyWorks team. Thus, the aerodynamics team explored alternatives to wind tunnel testing. This included the design and testing of a structural test fixture that can be mounted to the bed of a pickup truck. The stand includes four 1-axis force sensors oriented such that the values of lift, drag, and moments can be collected when the truck is in motion. The goals of the test were to verify the predicted aerodynamic forces and moments on the aircraft and jamming antenna that were obtained from CFD analysis. This test was scheduled to be completed at the end of February.

### 7.3.2 Static Propulsion Test

Static thrust tests were conducted on a thrust stand which recorded both force measurements and motor telemetry to evaluate propulsion package performance, as shown in Fig. 42. The thrust measurement stand was

constructed on a plywood base reinforced by 2x4 boards. The motor assembly was mounted on two pairs of linear bearings and connected to a load cell. An Arduino Nano was used to measure the thrust and log time-series data to a MicroSD card. After the motor was mounted, the Arduino was reset and a green LED indicated that the SD card was saving thrust data. The propulsion package can use a T-Motor AT4140 motor with 16X12E and 17X10E propellers, and 6S and 8S batteries for a total of four configurations. Testing procedures include maximum throttle tests to simulate take-off conditions and obtain static thrust data, and battery endurance tests in which the propulsion system is set to draw a predesignated amount of power to simulate M2.

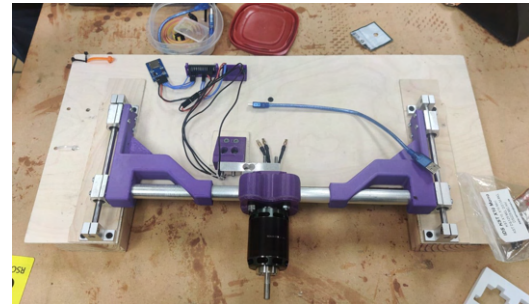


Figure 42: Thrust Test Stand

### 7.3.3 Materials Testing

#### 7.3.3.1 3-Point Bend Tests

To facilitate informed decision making, multiple materials tests were conducted. A preliminary test compared different densities of spread tow carbon fiber to find the optimal density for use on the final aircraft. For these tests, samples of 1.89 oz/yard<sup>2</sup>, 2.24 oz/yard<sup>2</sup>, 2.36 oz/yard<sup>2</sup>, 2.36 oz/yard<sup>2</sup> of 45°, 2.95 oz/yard<sup>2</sup>, and Innegra 3.38 oz/yard<sup>2</sup> spread tow fabrics were laid up on XPS foam core. These samples were loaded in a three point bending test and weight was applied. The edges of the beam were pinned at either end as they would be during GM.

#### 7.3.3.2 Instron Testing

In addition to the 3-point bend tests conducted, bending tests were also conducted using an Instron. A load was applied at two points along the material samples and gradually increased until failure. The samples tested were sandwich core panels. Samples with 2 ply of spread tow, 4 ply of spread tow, and 2 ply of prepreg were tested. Both honeycomb core and PVC foam core were tested for the spread tow samples; just honeycomb was tested for the prepreg, as the PVC foam core was not compatible for high-heat curing. The setup is shown in Fig.43.

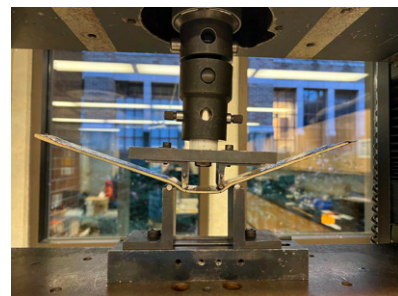


Figure 43: Instron Test Setup

#### 7.3.4 Mission 3 Antenna Adapter

To validate effectiveness, the adapter was tested by securing it to a table such that the PVC antenna was parallel to the ground. A bucket was then hung from the PVC pipe using a spring scale which measured the force applied as the bucket was filled with water. This concentrated load approximated the drag force the antenna would experience during level flight. The goal of this set-up was to observe how reliably the 3D printed adapter could hold the expected load without slipping or breaking. Adapters with heights of 0.6 in, 0.75 in, and 1.375 in were

tested. Weight was added to the aerodynamic center of the PVC antenna, either 12 in or 19 in from the end, depending on the antenna length. The target weight was 4.225 lb, which was the expected drag force at 131 ft/s.

### 7.3.5 Aircraft Assembly Time

In order to ensure that the aircraft can be assembled within five minutes, a time study was performed to analyze the bottlenecks during assembly and improve assembly time. The time study was performed by recording video of multiple people assembling the aircraft one at a time. Each person would assemble the aircraft multiple times with a different order of assembly. The goal of the time study was to determine the optimal strategy for aircraft assembly, determine the most time intensive processes, and build time stamps for the assembly time of each component. This process was iterated to minimizes assembly time.

### 7.3.6 Ground Mission

To ensure the safety of the GM loading process, the testing procedure will be performed in three steps. First, the V1 wing tip will be mounted to its anchor point on the ground test stand, and will be subjected to twisting and loading forces along the wing spar to ensure that there is no shearing at the mounting point. The aircraft will then be removed, and replaced with a 2x4 'spar', which will be loaded to simulate maximum loading conditions to ensure the test stands can withstand the weight without endangering the test aircraft. Finally, the V1 aircraft will be mounted and saddled with a weight platform, and will be carefully loaded incrementally with 20 lb and 40 lb sandbags to determine how much weight it can safely hold.

## 7.4 Flight Tests

### 7.4.1 Flight Test Aircraft

Three airworthy iterations of the *Sailfin* were built to test and improve various aspects of the design as detailed in Tables 22 and 23. Employing a phased approach to flight testing made it possible validate to aspects of the design one at a time and incorporate the lessons learned from flight tests onto the final competition aircraft. The goals of the aerodynamic prototype test flights were to simulate M1 and M3 and to understand the stability characteristics of the aircraft. The goal of the competition V1 aircraft was to practice manufacturing and integration, investigate the assembly time, and test all competition missions. Finally, the goal of the competition V2 aircraft was to integrate all that was learned from the previous two aircraft and have a competition-worthy build and design. Pictures of the aerodynamic prototype and competition V1 aircraft are shown in Fig. 44.

Table 22: Aircraft Tested

Production Order	Airframe	Description	First Flight
1	Prototype	Designed to be easy to build and was constructed out of cheap materials such as foam board and plywood. Used to test the aerodynamic performance of the aircraft in all three mission configurations.	1/14/23
2	Comp V1	First attempt at manufacturing a fully carbon fiber aircraft. This aircraft was used to validate the manufacturing process and ensure that the aircraft can fit in the box and be assembled and disassembled within the allotted 5 minutes.	2/15/23
3	Comp V2	The final, fully-functional competition aircraft incorporating design changes from lessons learned in the prototype and Competition V1 aircraft. Designed to operate off of a paved runway.	TBD

Table 23: Aircraft Features

Feature	Prototype	Competition V1	Competition V2
Fuselage Skin Material	Foam Board	Carbon Fiber	Carbon Fiber
Vertical Stabilizer Area	101.59 in <sup>2</sup>	142.04 in <sup>2</sup>	142.04 in <sup>2</sup>
Empennage Connection	Glued	Quick Connect	Quick Connect
Control Surface Servos	Conventional	IDS	IDS
Landing Gear Type	Grass	Grass	Pavement
Wing Locking Mechanism	Zip Ties	Friction Fit	Pin Lock
Motor	AT4130 300kV	AT4140 410kV	AT4140 410kV



(a) Aerodynamic Prototype



(b) Competition V1

Figure 44: Aircraft During Test Flights

### 7.4.2 Flight Test Schedule and Plan

Before each flight, the team used the checklist shown in Table 24 to validate that the aircraft was safe and ready to fly. Implementing a flight checklist reduces the inherent risk associated with flight tests. Alongside the checklist, Team HuskyWorks generated custom test plans for each test flight that covered the order of tests, goals, and what to do in case of failure during flight. The flight test plan is summarized in Table 25.

Table 24: Flight Checklist

PREFLIGHT		BEFORE TAKEOFF	
Assembly		Propeller Area	CLEAR
Empennage	SECURE	Throttle Inhibit Switch	OFF
Wings	SECURE	Aircraft	RESTRAIN
Horizontal Stabilizer	SECURE	Throttle	RUN UP TO 80%
Landing Gear	SECURE	Control Surfaces	FREE AND CORRECT
Motor	SECURE	Flaps	AS REQUIRED
Flight and Avionics Batteries	SECURE	Control Throw	LOW RATES
Center of Gravity	1/4 CHORD	Takeoff Area	CLEAR
Propeller	TIGHTENED	Takeoff Intentions	ANNOUNCED
Avionics		TX Battery	CHECKED
Throttle Inhibit Switch	ON	Timer	START
Transmitter	ON	BEFORE LANDING	
Receiver Connections	INSPECTED	Flaps	DOWN
Avionics Battery Voltage	CHECKED	Landing Area	CLEAR
Flight Battery Voltage	CHECKED	Landing Intentions	ANNOUNCED
Avionics Battery	CONNECTED	AFTER LANDING	
Flight Battery	CONNECTED	Throttle Inhibit Switch	ON
Avionics Battery	SECURE	Timer	STOP
Flight Battery	SECURE	Flight Battery	DISCONNECT
Flight Data	RECORDING	Avionics Battery	DISCONNECT
Battery Access Hatch	CLOSED	Avionics Battery Voltage	CHECKED
Failsafe (1st Flight of Day)	CHECKED	Flight Battery Voltage	CHECKED
Range (1st Flight of Day)	CHECKED	Radio Power	OFF
Airframe		Aircraft Structure	INSPECT
Payload	SECURE		
Payload Access Hatch	CLOSED		
Landing Gear Roll	SMOOTH		
Control Surfaces	SECURE		
Control Inputs	CORRECT		
Trims	CORRECT		

Table 25: Flight Test Plan

Flight	Date	Airframe	Objectives	Completed
1	1/14/23	Prototype	- Trim aircraft for comfortable cruise with and without flaps - Analyze aircraft stability in cruise flight	Yes
2	1/14/23	Prototype	- Verify aircraft yaw stability with modified rudder - Trim aircraft for approach speed with flaps down - Practice approaches to predict landing behavior - Estimate power draw from remaining battery voltage	Yes
3	1/14/23	Prototype	- Test stall characteristics with flaps up, takeoff flaps - Test high speed performance - Observe live stall, cruise, maximum, and landing speeds	Yes
4	1/14/23	Prototype	- Demonstrate pitch and yaw stability with 1 ft PVC antenna - Verify control at cruise and landing speed with 1 ft antenna - Practice approaches with 1 ft antenna	Yes
5	1/14/23	Prototype	- Demonstrate pitch and yaw stability with 2 ft PVC antenna - Verify control at cruise and landing speed with 2 ft antenna - Practice approaches with 2 ft antenna	Yes
6	1/14/23	Prototype	- Demonstrate pitch and yaw stability with 39 in PVC antenna - Verify control at cruise and landing speed with 39 in antenna - Practice approaches with 39 in antenna	Yes
7	1/22/23	Prototype	- Practice landings with flaps deployed - Observe ground roll using landing flap setting	Yes
8	1/22/23	Prototype	- Observe flight handling with 1.5 lb payload - Practice stalls with 1.5 lb payload - Practice landing with 1.5 lb payload	Yes
9	1/22/23	Prototype	- Observe flight handling with 3 lb payload - Practice stalls with 3 lb payload - Practice landing with 3 lb payload	Yes
10	2/15/23	Comp V1	- Trim aircraft at all flap settings - Practice approaches and landings	Yes
11	2/23/23	Comp V1	- Demonstrate flight with 2 ft PVC antenna	Yes
12	2/23/23	Comp V1	- Demonstrate flight with 39 in PVC antenna - Practice competition laps with 39 in PVC antenna	Yes
13,14,15,16	2/23/23	Comp V1	- Demonstrate flight with 3 lb, 6 lb, 9 lb and 12 lb M2 payloads - Verify that aircraft is controllable at each weight - Verify that aircraft can take off within 60 ft at max payload	Yes
16,17,18	TBD	Comp V2	- Practice mission laps in M1 configuration - Practice approaches and landings in M1 configuration	No
19,20,21	TBD	Comp V2	- Practice mission laps in M2 configuration - Practice approaches and landings in M2 configuration - Practice laps at various M2 payload weights to optimize score	No
21,22,23	TBD	Comp V2	- Practice mission laps in M3 configuration - Practice approaches and landings in M3 configuration - Practice competition laps to optimize lap speed	No

## 8 Performance Results

The following sections detail the performance results of the *Sailfin* and sub-system testing conducted on the ground and in flight.

### 8.1 Demonstrated System Performance

The performance results of all sub-systems are detailed in the following sections. Aerodynamic, assembly time, and GM tests are scheduled for late February and early March, thus their data has yet to be collected and is not included. Through sub-system testing, the motor and structural performance of the aircraft and aircraft components were validated; additionally, materials were chosen for the fuselage and wings.

#### 8.1.1 Static Propulsion Test

Static thrust tests were conducted to validate performance and maximize mission scores. To find the optimal propellers for each flight mission, the APC 16X12E and 17X10E propellers were evaluated using the T-Motor AT4140 410KV motor and the SMC 8S 3200 mAh 75C battery. Thrust and motor RPM data points were taken while operating at mission power limits prescribed by Eq. 6 on the battery. Then, dynamic thrust at mission flight speeds were calculated based on APC's official performance data sheet. As seen in Table 26, the 16X12E propeller is superior in flight while providing sufficient takeoff thrust. However, noting that propellers tend to obtain higher RPM in flight than during static tests, the 16X12E propeller was selected as the primary propeller, with further validation required by flight testing. As seen in Table 26, the 16X12E propeller is superior in flight while providing sufficient takeoff thrust. However, noting that propellers tend to obtain higher RPM in flight than during static tests, the 16X12E propeller was selected as the primary propeller, with further validation required by flight testing.

Table 26: Static Propulsion Test Results

Propeller	M2 RPM	M2 Flight Thrust (lb)	Max RPM	Max Static Thrust (lb)	M3 RPM	M3 Flight Thrust (lb)
APC 16X12E	~5000	1.3	8914	15.2	~8000	5.7
APC 17X10E	~5000	0.3	8829	18.3	~8000	3.1

Additionally, fuses were evaluated during durability tests to establish safe operating parameters. Throttle was advanced to max on a full battery to produce maximum load on the fuse, and time was recorded from setting max throttle to fuse failure. Over multiple tests, the average time was approximately 17 seconds. With a factor of safety accounting for variables such as temperature, the max throttle time limit was set to 12 seconds. Finally, an M2 simulation test was conducted by discharging a full battery at the M2 average power limit. In order to protect the battery for future testing, the battery was only discharged for the M2 time window of 10 minutes. From this test, the battery was proved to be capable of discharging at 507 Watts for the duration of the mission window. With cells resting at 3.7V, it was deduced that there could be sufficient energy for the pilot to perform the landing lap.

### 8.1.2 Materials Testing

Material testing yielded results for strength-to-weight of materials during the 3 point bend tests, and a load vs deflection for the Instron testing. 3 point bend testing concluded that the material with the highest strength-to-weight ratio was the two fabrics that weighed 2.36 oz/yd<sup>2</sup>. This was chosen with fibers oriented at 45° with respect to the wings. The angle was chosen to provide maximum torsional resistance for flutter at the wing tips and for the antenna flight. Instron testing yielded results used in selecting the fuselage material. It was determined that the material that could take the most load with minimal deflection were the prepreg-honeycomb sandwich coupons. It was determined that the 2 ply sandwich had sufficient strength for the nose and empennage sections, while 4 ply was needed for the non-tapered section of the fuselage and the empennage connection point. The results from the Instron testing are summarized in Fig. 45.

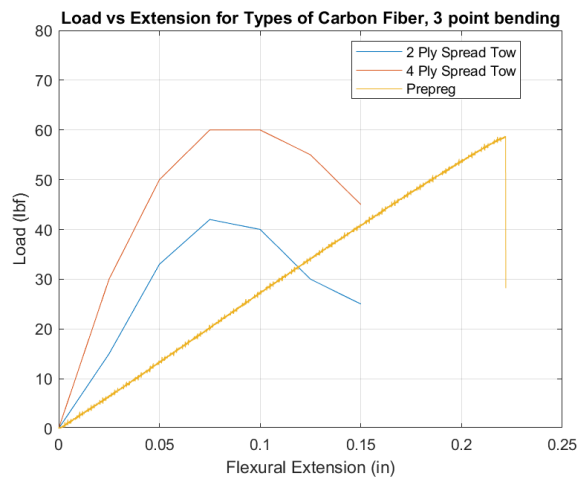


Figure 45: Instron Testing Graphical Data

### 8.1.3 Mission 3 Antenna

The M3 testing results showed that the 0.6 in adapter was the optimal balance between strength and minimizing height. The 1.5 in adapter was able to hold 10.50 lb at 12 in without any noticeable deformation, which indicated it was over-engineered and could be far shorter without failing at the target of 5.6 lb. The next experiment tested a 0.5 in adapter which displayed a loss of traction at 5.90 lb and shattered at 6.10 lb at the same distance. While this technically met the target strength, the margin-of-error was considered too small by the HuskyWorks team. 0.6 in and 0.75 in adapters were also tested. The 0.6 in iteration held 8.80 lb 12 in from the adapter before failure, and showed no slippage before this point. This weight corresponds to 187 ft/s flight, which is an acceptable factor of safety for the mission. When the weight was shifted to 19 in, the adapter held 6.38 lb without any issues. This weight corresponds to 131.7 ft/s flight, which is an acceptable factor of safety for the mission.

Table 27: Antenna Adapter Test Results

Adapter Height	Force Applied (lbs)	Equivalent Velocity (ft/s)	Simulated Drag Direction	Qualitative Notes
0.6	5.6	150.82	Chord-wise	Noticeable bending in PVC pipe, stable adapter with no slipping
0.6	6.38	160.98	Chord-wise	Severe pipe bending, no slipping at adapter
0.6	2.92	N/A, tested turning flight	Span-wise	Some pipe bending, stable adapter with no slipping
0.75	5.62	151.09	Chord-wise	Some bending and a little slippage, but no cracks formed
0.75	3.53	N/A, tested turning flight	Span-wise	Mild bending and no slippage or damage
1.375	10.5	206.52	Chord-wise	Significant pipe bending, but adapter was unaffected

## 8.2 Flight Performance

### 8.2.1 Flight Test Outcomes

Table 28 details the observations and outcomes from each flight of the test program. Lessons learned from each aircraft iteration were applied to subsequent aircraft. During test flights, telemetry data including airspeed, attitude and load factor were down linked live to a headset worn by a ground crew member. Table 29 details predicted values with those observed during the test flight. Fig. 46 and 47 show pictures of the competition V1 aircraft on takeoff and in flight.

Table 28: Flight Test Results

Flight	Airframe	Duration	Observations	Outcomes
1	Aero Prototype	1:14	First flight of aerodynamic prototype. Flight was cut short due to undesirable oscillatory yawing motion induced by rudder with excessive area in front of the hinge point. Successful no flap landing was conducted.	- Rudder area in front of the hinge point was cut down to eliminate the yaw oscillations
2	Aero Prototype	6:25	First flight with modified rudder. Yaw oscillations were eliminated by the modification. Aircraft trimmed for cruise flight. Practice laps to familiarize pilot with aircraft handling characteristics. Aircraft landed with excessive forward speed and no flaps which led to a runway overrun which broke off the main landing gear.	- Landing gear was repaired and modified to be more robust - Future landings conducted with full flaps to increase lift and drag and reduce float behavior in ground effect
3	Aero Prototype	~8m	Envelope expansion flight. Stalls with and without flaps were conducted to determine stall characteristics. High speed passes conducted to determine high speed handling characteristics.	- Observed stall behavior helped pilot to determine best methodology for conducting safe landings
4	Aero Prototype	~4m	Flight with 1 ft antenna. Aircraft was stable in pitch with only a small amount of yaw towards the antenna.	- Flight allowed pilot to gain experience flying with a short antenna before moving to longer antenna lengths.
5	Aero Prototype	~5m	Flight with 2 ft antenna. Aircraft pitched up abruptly on takeoff but was stable in the pitch axis in flight. Yaw towards antenna was significantly higher but could be overcome with opposite rudder.	- Pilot gained experience with medium length antenna before moving to the competition antenna length - Subsequent takeoffs were conducted with less up elevator to mitigate pitch up on takeoff
6	Aero Prototype	~4.5m	Flight with 39 in antenna. Aircraft was stable in pitch and yaw but could not achieve coordinated flight due to the larger asymmetric drag from antenna even with full opposite rudder deflection.	- The vertical stabilizer design for the competition aircraft was resized to improve yaw authority
7	Aero Prototype	~8m	Practice landings and competition laps.	- Pilot became more proficient flying aircraft
8	Aero Prototype	~4m	Flight with 1.5 lb M2 payload. Aircraft flew nominally and pilot noticed no significant changes in behavior from empty weight.	- Flight allowed pilot to gain experience flying with higher wing loading in preparation for larger payloads
9	Aero Prototype	~2m	Flight with 3 lb M2 payload. Aircraft handling characteristics were nominal. The empennage severed from the aircraft in a high-g turn resulting in a crash.	- The fuselage empennage joint was redesigned for the competition aircraft to increase its durability
10	V1	~7m	First flight of Comp V1 aircraft. Rudder deflected due to loose rudder cable.	- Rudder cables tightened and rudder control horn reinforced with epoxy
11	V1	5:22	Airspeed data collection flight. Speeds recorded during high speed passes, stalls, approaches and cruise flight.	- Airspeed data compared with analytical airspeed calculations to validate performance predictions
12	V1	7:02	Flight with 3 lb M2 payload. Aircraft handled well in the air. Landing gear was bent in hard landing.	- Landing gear design improved to transfer load more effectively to fuselage
13	V1	4:05	First flight with 6 lb M2 payload. Aircraft handled well. Approach speed was increased to account for the increased wing loading.	- A rough baseline of the power consumption for M2 was established - Baseline M2 weight was established

Table 29: Demonstrated Flight Performance

Parameter	Flight Test	Analytical Prediction
Empty Weight (lb)	9.25	10.61
Maximum Observed Load Factor	4.2	-
Flight Endurance (min)	9:17	10:00
Cruise Airspeed (ft/s)	68.3	82.0
Max Demonstrated Speed (ft/s)	132.2	131.0
Stall Airspeed (ft/s)	31.9	30.6
Approach Airspeed (ft/s)	41.0	39.8



Figure 46: V1 Competition Aircraft Takeoff



Figure 47: Competition V1 Flying M2 Simulation

### 8.2.2 Design Modifications Motivated by Flight Tests

The flight test program resulted in modifications to both the aerodynamics and structure of the aircraft. The primary changes were motivated by observations from the flight tests of the aerodynamic prototype. The original design of the aerodynamic prototype featured a very short nose to help the aircraft fit in the box. However, after manufacturing was completed, it was discovered that a fuselage extension was necessary to achieve the desirable aircraft CG. This modification was made before the first test flight and was carried over to the design for the competition aircraft as well. During flight tests with the 39 in antenna on the prototype, the pilot noted that the aircraft did not have sufficient yaw authority to counteract the yaw induced by the antenna. Consequently, the size of the vertical stabilizer and rudder were increased, which increased the vertical tail volume coefficient. Additionally, during an M2 simulation with a 3 lb payload, the empennage severed from the fuselage after multiple high-g turns. This prompted a redesign of the fuselage-to-empennage joint for the competition aircraft to improve its structural integrity. The competition V1 aircraft was used to evaluate M2 performance for higher payload weights. The aircraft flew well with 3 lb and 6 lb M2 weights, however when the aircraft was loaded with the 9.33 lb payload, the center spar buckled during a wingtip loading test on the ground. An analysis was conducted on the failure, and optimizations were made on the material design of the spar and the manufacturing process.



Figure 48: Competition V1 Flight Test Crew

## References

- [1] "2022-23 Design, Build, Fly Rules," 2022.
- [2] MATLAB, *version 10.10.0 (R2022a)*, The MathWorks Inc., Natick, Massachusetts, 2022.
- [3] OpenVSP, National Aeronautics and Space Administration, 2020.
- [4] Muller, M., *ecalc*, ecalc, 2022.
- [5] SOLIDWORKS 2021, Dassault Systemes, 2020.
- [6] Deperrios, A., *XFLR5*, 2021.
- [7] Drela, M., *AVL*, Massachusetts Institute of Technology, 2020.
- [8] Raymer, D., *Aircraft Design: A Conceptual Approach*, American Institute of Aeronautics and Astronautics, Inc., 6th ed., 2018.
- [9] Drela, M., *XFOIL 6.99*, Massachusetts Institute of Technology, 2020.
- [10] Anderson, J., *Introduction to Flight*, McGraw-Hill Education, New York, NY, 8th ed., 2016.
- [11] ANSYS Student, Ansys Inc., 2020.
- [12] Bruhn, E. F., *Analysis and Design of Flight Vehicle Structures*, Tri-State Offset Company, 1973.